CD148 Deficiency in Fibroblasts Promotes the Development of Pulmonary Fibrosis

Konstantin Tsoyi[1], Xiaoliang Liang[1], Giulia De Rossi[2], Stefan W. Ryter[3], Kevin Xiong[4], Sarah G. Chu[4], Xiaoli Liu[4], Bonna Ith[4], Lindsay J. Celada[1], Freddy Romero[1], Matthew J. Robertson[1], Anthony J. Esposito[4], Sergio Poli[4], Souheil El-Chemaly[4], Mark A. Perrella[4], YuanYuan Shi[5], James Whiteford[2] and Ivan O. Rosas[1,4]*

[1]Section of Pulmonary, Critical Care and Sleep Medicine, Department of Medicine, Baylor College of Medicine, Houston, Texas, USA.

[2]William Harvey Research Institute, Barts and the London School of Medicine and Dentistry, Queen Mary University of London, London, UK.

[3]Division of Pulmonary and Critical Care Medicine, Department of Medicine, Weill Cornell Medicine, New York, New York, USA.

[4]Division of Pulmonary and Critical Care Medicine, Department of Medicine, Brigham and Women's Hospital, Harvard Medical School, Boston, Massachusetts, USA.

[5]School of Life Sciences, Beijing University of Chinese Medicine, Beijing, China.

*Corresponding Author:

Ivan O. Rosas, M.D. Section of Pulmonary, Critical Care and Sleep Medicine.

Department of Medicine. Baylor College of Medicine. 7200 Cambridge Street. Houston, TX, 77030. Email: ivan.rosas@bcm.edu

Running Head: Antifibrotic effects of CD148 in IPF

Descriptor: 3.1

Total Word Count: 4,047

This article has an online data supplement, which is accessible from this issue's table of content online at www.atsjournals.org

At a Glance Commentary

Scientific Knowledge on the Subject:

Idiopathic pulmonary fibrosis (IPF) is a pulmonary disease involving fibrotic changes of the lung with unknown etiology, for which there is no cure. The pathogenesis of IPF involves dysregulated wound healing, damage to lung epithelium, fibroblast/myofibroblast activation and excessive extracellular matrix production, leading to aberrant lung remodeling. The receptor-like protein tyrosine phosphatase eta (CD148) exerts anti-fibrotic effects in experimental pulmonary fibrosis *via* interactions with its ligand syndecan-2; however, the role of CD148 in fibroblast activation remains unknown.

What This Study Adds to the Field:

In this study, we demonstrate that CD148 expressed in lung fibroblasts can confer antifibrotic effects in human and experimental pulmonary fibrosis. CD148-deficient fibroblasts exhibited hyperactivated PI3K/Akt/mTOR signaling, reduced autophagy and increased p62 accumulation, leading to NF-κB activation, which we identify as a novel mechanism regulating profibrotic gene expression. CD148-targeting peptides can exert anti-fibrotic effects and show therapeutic potential in experimental and human fibrosis.

Abstract

Rationale: The receptor-like protein tyrosine phosphatase eta (CD148/PTPRJ) exerts anti-fibrotic effects in experimental pulmonary fibrosis *via* interactions with its ligand syndecan-2; however, the role of CD148 in human pulmonary fibrosis remains incompletely characterized.

Objectives: We investigated the role of CD148 in the profibrotic phenotype of fibroblasts in idiopathic pulmonary fibrosis (IPF).

Methods: Conditional CD148 fibroblast-specific knockout mice were generated and exposed to bleomycin, and then assessed for pulmonary fibrosis. Lung fibroblasts (mouse lung, and human IPF lung), and precision cut lung slices (PCLS) from human IPF patients were isolated and subjected to experimental treatments. A CD148-activating 18-aa mimetic peptide (SDC2-pep) derived from syndecan-2 was evaluated for its therapeutic potential.

Measurements and Main Results: CD148 expression was downregulated in IPF lungs and fibroblasts. In human IPF lung fibroblasts, silencing of CD148 increased extracellular matrix production and resistance to apoptosis, whereas overexpression of CD148 reversed the profibrotic phenotype. CD148 fibroblast-specific knockout mice displayed increased pulmonary fibrosis after bleomycin challenge compared to control mice. CD148-deficient fibroblasts exhibited hyperactivated PI3K/Akt/mTOR signaling, reduced autophagy and increased p62 accumulation, which induced NF-κB activation and profibrotic gene expression. SDC2-pep reduced pulmonary fibrosis *in vivo*, and inhibited IPF-derived fibroblast activation. In PCLS from IPF and control patients, SDC2-pep attenuated profibrotic gene expression in IPF and normal lungs stimulated with pro-fibrotic

stimuli.

Conclusions: Lung fibroblast CD148 activation reduces p62 accumulation, which exerts anti-fibrotic effects by inhibiting NF-κB mediated profibrotic gene expression. Targeting the CD148 phosphatase with activating ligands such as SDC2-pep may represent a potential therapeutic strategy in IPF.

Abstract: 250 words

Keywords: **CD148, Fibroblast, Idiopathic pulmonary fibrosis, Nuclear Factor-kappa-B, Syndecan-2**

Introduction

Idiopathic pulmonary fibrosis (IPF) is a chronic, progressive lung disease characterized by lung scarring (1). The incidence of IPF is age-dependent, and has a high rate of mortality, with a median survival of three years (1). The pathogenesis of IPF involves dysregulated wound healing with continuous damage to lung epithelium, fibroblast/myofibroblast activation and excessive extracellular matrix (ECM) production, leading to aberrant lung remodeling (2). Since activated fibroblasts and myofibroblasts are among the key effectors of organ fibrogenesis, determining the molecular mechanisms underlying their pro-fibrotic phenotype may accelerate therapeutic development in IPF (2). Although existing antifibrotic therapies can slow progression of the disease (3, 4), none can reverse existing fibrosis. Thus, there remains an urgent unmet need to identify new therapeutic targets in IPF.

The receptor-like protein tyrosine phosphatase-eta (PTPRJ/CD148) is expressed throughout the hematopoietic system and in the lung, pancreas, thyroid, kidney, mammary glands and nervous system. CD148 consists of 1,337 amino acids with a single phosphatase domain containing the conserved motif (I/V)HCXAGXGR(S/T)G common to protein tyrosine phosphatases (PTPs) (5). CD148 can regulate cell proliferation, apoptosis, migration and invasion in multiple cancers (6-8). CD148 can dephosphorylate and inactivate proteins that regulate mitogenic signals (i.e., PDGF, EGF and VEGF) and act as a putative negative regulator of growth factor receptor signaling, *via* PTP activity (9, 10). Moreover, CD148 can negatively regulate PI3K/Akt signaling by dephosphorylating p85 (the regulatory subunit of PI3K) (11, 12). Hyperactivation of PI3K signaling and shared phenotypes between profibrotic fibroblasts derived from IPF lung and cancer cells (*e.g.,* increased invasiveness, migration and resistance to cell death) suggest a contributory role of CD148 in IPF (13-15). Here, we sought to delineate the mechanism(s) by which CD148 regulates fibroblast activation and its role as a therapeutic target in IPF.

Syndecans (SDCs) are cell surface heparan sulfate proteoglycans that regulate many cellular functions including proliferation, migration, and cell survival (16). We have shown that syndecan-2

(SDC2), a ligand of CD148, is highly expressed in IPF lungs and alveolar macrophages (AMs) (17). Transgenic overexpression of SDC2 or treatment with SDC2 attenuated experimental lung fibrosis *via* CD148 (18), which is consistent with experimental reports in endothelial and T-cells (19-20). However, the precise role of fibroblast CD148 in the pathogenesis of human pulmonary fibrosis is largely unexplored. Some of the results of these studies have been previously reported in the form of an abstract (21).

Methods

Primary Pulmonary Fibroblasts

The institutional review board at Brigham and Women's Hospital approved all experiments. Lung fibroblasts were isolated from lung transplantation recipients with IPF or nonfibrotic lungs. Mouse lung fibroblasts were isolated as described (22). Fibroblasts were cultured in DMEM media containing 10% FBS and antibiotics (Corning) in humidified incubators at 37°C and 10% CO_2. To induce Cre recombinase expression in $Ptprj^{fl/fl}$/ Col1a2-Cre-ER(T)$^{+/0}$ or Col1a2-Cre-ER(T)$^{+/0}$ lung fibroblasts, cells were treated with 4-hydroxytamoxifen (4-OHT, 1 μM).

Mice

All protocols were approved by the Brigham and Women's Hospital Standing Committee for Animal Welfare. C57BL/6 mice (Charles River) were used at 8 weeks of age. GFP-LC3 transgenic mice were described (23). To generate fibroblast-specific CD148-knockout mice, transgenic Col1a2$^{Cre-ER(T)+/0}$ and $Ptprj^{fl/fl}$ mice which possess loxP sites on both sides of exon 18, a transmembrane domain of $Ptprj$ (Jackson Laboratory) were crossbred. $Ptprj^{fl/fl}$ Col1a2$^{Cre-ER(T)+/0}$ mice (8–10 weeks old) or control Col1a2$^{Cre-ER(T)+/0}$ mice were administered tamoxifen (75 mg/kg, *i.p.*) for 5 days before experimental treatments and every 72 h until sacrifice (Figure E11).

Bleomycin model of pulmonary fibrosis

Lung fibrosis was elicited in mice by BLM (0.75 mg/kg, intratracheal) (Cayman Chemical); control mice received an equal volume of saline. Mice were sacrificed 21 days after BLM instillation. BAL

fluids were analyzed for immune cell counts. The left lung was analyzed for hydroxyproline (18). The right lung lobes were assessed for gene expression and histology.

SDC2-ED 18-aa peptide (SDC2-pep) administration

SDC2-ED 18-aa peptide (SDC2-pep, 0.5 mg/kg in 50 µl PBS) or PBS (vehicle) was administered at days 10, 12, 14, 16 and 18 post-BLM or saline treatment in mouse strains by intranasal instillation. Mice were sacrificed at day 24.

Precision Cut Lung Slices (PCLS)

PCLS from control and IPF lungs were prepared as described (24, 25), and transfected with scr, shCD148, EV or pLenti-GIII-CD148-HA lentiviral particles (1~1.5 MOI per slice). 12 h later, PCLS were incubated ± SDC2-pep (5 µM) for 72 h. PCLS were subjected to immunofluorescent staining or gene expression analysis.

Histopathology and Immunofluorescent co-staining

Human lung sections were fixed and immunostained for α-SMA and CD148. Mouse lungs were collected on Day 21 after BLM and stained with hematoxylin and eosin (H+E) or Masson's trichrome. See Supplementary Methods for details.

Transfection, **gene expression, and cellular assays**

Lung fibroblasts were stably transfected with either shRNA targeting CD148 (SigmaAldrich) or expression plasmid containing CD148 cDNA (ABMgood) by standard methods. Transient transfection assays were performed using FuGENE 6 transfection reagent (Promega) (26). Immunoblot and qPCR analyses (27), and gel contraction assays (18) were performed as described. Cell viability was determined using 3-[4,5-dimethylthiazol-2-yl]-2,5-diphenyl tetrazolium bromide (MTT) and trypan blue exclusion assays as described (26). Caspase-3 activity was measured using a kit (#K006-100, Biovision). See Supplementary Methods for details.

Statistical analysis

Data are expressed as mean ± SEM. Kaplan-Meier survival curves were analyzed by log-rank tests to assess for differences in survival. For comparisons between two groups, we used Student's unpaired t test or Mann-Whitney's non-parametric test. Statistical significance was defined as P<0.05. One-way analysis of variance, followed by Newman-Keuls or Tukey's post-test analysis or Kurskal-Wallis non-parametric test, was used for analysis of more than two groups.

Results

CD148 is downregulated in IPF

We measured the expression of CD148 in IPF or control lungs and in cell isolates from these lungs. CD148 protein and corresponding *Ptprj* mRNA levels were downregulated in IPF lungs compared to control lungs (Figure 1, A-B). In IPF lung homogenates enriched for fibroblasts (Figure E1) (28), *Ptprj* mRNA was downregulated relative to fibroblast-enriched control lung homogenates (Figure 1C). Immunofluorescence staining revealed that CD148 co-stained with vimentin-positive cells in control lungs, indicating its expression in fibroblasts, whereas CD148 staining was significantly reduced in IPF lungs (Figure 1D). Co-staining of IPF lungs with αSMA and CD148 confirmed that CD148 is downregulated in myofibroblasts (Figure E2A). Analysis of a previously reported single cell RNA sequencing (scRNAseq) dataset for IPF lung (29) revealed downregulated CD148 gene expression in IPF myofibroblasts compared to controls, which did not achieve statistical significance (Figure E3). CD148 gene expression was modestly increased in IPF fibroblasts compared to control fibroblasts (Figure E3). Finally, we determined that CD148 was also expressed in alveolar epithelial type I and type II (AT1 and AT2) cells from control lungs (Figure E2B), with reduced staining (Figure E2B) and lower mRNA expression (Figure E4A) in AT2 cells from IPF lungs.

CD148 regulates the profibrotic phenotype of lung fibroblasts derived from IPF patients

Fibroblasts isolated from IPF lungs have increased ECM production and resistance to cell death and apoptosis (30-32). To determine the role of CD148 in fibroblasts isolated from IPF lungs, we silenced CD148 expression in these cells using shCD148 (Figure 1E). CD148 silencing resulted in higher gene expression of fibronectin (*Fn*) and collagen 1a1 (*Col1a1*) in IPF-derived lung fibroblasts relative to scramble (scr)-transfected IPF fibroblasts (Figure 1F). Furthermore, IPF fibroblasts were resistant to cell death induced by Fas ligand (FasL) (Figure E4B). This effect was enhanced in CD148-deficient cells (Figure 1G). Overexpression of CD148 using stable lentiviral transduction with pLenti-CD148-HA (Figure 1H) resulted in downregulation of ECM gene expression (*Fn, Col1a1*) (Figure 1I), increased cell death (Figure 1J) and enhanced caspase-3 activity (Figure E4C).

CD148 deficiency in fibroblasts leads to increased pulmonary fibrosis in bleomycin (BLM)-challenged mice

To investigate the role of CD148 in pulmonary fibrosis, we generated mice with a fibroblast-specific conditional deletion of CD148 (*Ptprj*$^{fl/fl}$ Col1a2$^{Cre-ER(T)+/0}$). CD148 was deleted in lung fibroblasts isolated from tamoxifen-treated *Ptprj*$^{fl/fl}$ Col1a2$^{Cre-ER(T)+/0}$ mice (Figure E5A). We exposed *Ptprj*$^{fl/fl}$ Col1a2$^{Cre-ER(T)+/0}$ mice or Col1a2$^{Cre-ER(T)+/0}$ (control) mice to BLM to induce pulmonary fibrosis. At 21 days following BLM instillation, *Ptprj*$^{fl/fl}$ Col1a2$^{Cre-ER(T)+/0}$ mice displayed greater lung interstitial thickening compared to control mice (Figure E5B). The fibroblast-specific CD148 deficient mice also displayed markedly higher lung collagen content, by Masson's Trichrome stain (Figure 2A) and hydroxyproline measurements (111.8$\pm$18.5 *vs.* 80.8$\pm$8.8 µg/ml/lobe) (Figure 2B), reduced survival (Figure 2C), higher lung expression of α-SMA (Figure 2, D-E) and profibrotic genes (*Fn, Col1a1,* and *Ctgf*) (Figure 2, F-G) and reduced CD148 expression (Figure 2, D-E). There was no difference in inflammatory cell counts in the bronchoalveolar lavage (BAL) fluid between the strains after BLM challenge (Figure E5C).

CD148 deficiency leads to increased myofibroblast differentiation, ECM production and resistance to apoptosis in fibroblasts after TGF-β1 stimulation

Lung fibroblasts from *Ptprj*$^{fl/fl}$ Col1a2$^{Cre-ER(T)+/0}$ and Col1a2$^{Cre-ER(T)+/0}$ (control) mice were isolated. CD148 deficiency enhanced TGF-β1-induced myofibroblast differentiation, as determined by α-SMA expression (Figure 2H) and increased the ECM gene expression (*Col1a1* and *Fn*) (Figure 2I). Cell contractility was higher in *Ptprj*$^{-/-}$ fibroblasts compared to wild type cells after TGF-β1 treatment (Figure 2J). TGF-β1 stimulation induced resistance to FasL-induced cell death and apoptosis in wild-type cells, which was exacerbated in *Ptprj*$^{-/-}$ fibroblasts (Figure 2K). CD148 deficiency also increased cell proliferation induced by TGF-β1 in fibroblasts (Figure E5D).

CD148 deficiency upregulates TGF-β1-induced PI3K/Akt/mTOR signaling

CD148 regulates PI3K signaling by dephosphorylating (inactivating) the regulatory subunit of PI3K (p85) (11). As PI3K/Akt signaling is upregulated in activated fibroblasts and contributes to the development of pulmonary fibrosis (13, 15, 33), we investigated whether CD148 deficiency can enhance PI3K/Akt/mTOR signaling induced by TGF-β1 in lung fibroblasts derived from *Ptprj*$^{fl/fl}$ Col1a2$^{Cre-ER(T)+/0}$ mice. TGF-β1 treatment upregulated the phosphorylation of PI3K (p85 subunit), Akt, mTOR and mTOR-related signaling proteins (p70 S6-kinase and S6) (Figure 3A). CD148 deficiency further increased the expression of phospho (p)-PI3K, p-Akt, p-mTOR, and downstream targets, p-p70 and p-S6 (Figure 3A, and Figure E6A).

CD148 deficiency inhibits autophagy and leads to p62 accumulation in lung fibroblasts

Activation of mTOR suppresses autophagy in IPF-derived fibroblasts (30). As the absence of CD148 leads to activation of mTOR, a regulator of autophagy, we hypothesized that CD148 deficiency could potentially modulate autophagy. TGF-β1 downregulated autophagy in lung fibroblasts, as reflected by reduced expression of microtubule associated protein-1 light chain-3B (LC3)-II (active form) relative to LC3-I, and increased p62 expression (Figure 3B and Figure E6, B-D). CD148 deficiency exacerbated the suppression of autophagy by TGF-β1 (Figure 3B). We

also examined relative autophagic flux using LC3 turnover assay. Wild type and *Ptprj*^{-/-} fibroblasts were treated with chloroquine which inhibits autophagosome-lysosome fusion and consumption of LC3B; this causes an accumulation of LC3-II that reflects the rate of autophagosome formation in the presence or absence of TGF-β1. CD148 deficient fibroblasts exhibited delayed LC3-II accumulation compared to control fibroblasts (Figure 3C and Figure E6E). Decreased autophagosome formation was also observed in LC3-GFP transgenic lung fibroblasts in the absence of CD148 (Figure 3, D-E). We next investigated whether the PI3K/mTOR axis and p62 upregulation are essential for the pro-fibrotic response in CD148 deficient cells. We found that increase of α-SMA in CD148-deficient cells in response to TGF-β1 was attenuated by wortmannin (a PI3K inhibitor), rapamycin (an mTOR inhibitor) and by p62 knockdown using sh-p62 (Figure E7).

p62-dependent NF-κB activation drives transcriptional regulation of profibrotic gene expression

In cancer cells, p62 accumulation activates NF-κB by phosphorylating the inhibitor of kappa-B kinase (IKK), resulting in degradation of the kappa-B inhibitor (I-κB) and NF-κB nuclear translocation (34, 35). We thus sought to determine the relevance of this pathway in fibrogenesis. CD148-deficient cells (*Ptprj*^{-/-}) had higher levels of p-IKKα/β and p-I-κB (Figure 4A), and higher nuclear accumulation of NF-κB (p65 subunit) (Figure 4B) in response to TGF-β1. In CD148-deficient lung fibroblasts, *Col1a1* and *Acta2* mRNA expression levels were dependent on PI3K/Akt, mTOR and p62 levels in response to TGF-β1 (Figure 4, C-D). Interestingly, NF-κB activity in CD148-deficient cells was also dependent on PI3K/Akt, mTOR and increased p62 levels (Figure 4E). The NF-κB inhibitor Bay 11-7082 inhibited TGF-β1-dependent increase in *Col1a1* expression in CD148-deficient cells (Figure 4F). Taken together, we demonstrate for the first time that decreased autophagy may transcriptionally modulate profibrotic gene expression by enhancing a p62/NF-κB signaling axis. Furthermore, we demonstrate that CD148 counteracts this

signaling axis by inhibiting the PI3K/Akt/mTOR pathway. We also further confirmed the role of CD148 in regulating this pathway by overexpressing CD148 in human lung fibroblasts. As shown in Figure E8, overexpression of CD148 attenuated p62, p-IKKα/β, p-I-κB expression and inhibited NF-κB luciferase activity in response to TGF-β1.

An 18-aa SDC2-ED derived peptide (SDC2-pep) inhibits pulmonary fibrosis via CD148 in vivo and in vitro

Two known extracellular proteins, thrombospondin and SDC2, can bind to CD148 and activate PTP activity (20, 36). Furthermore, we have previously identified an 18-aa sequence of the SDC2 ectodomain responsible for binding and activation of CD148 in endothelial cells (19, 20). We therefore evaluated the therapeutic potential of a SDC2-peptide (SDC2-pep) in the mouse model of BLM-induced fibrosis. We exposed *Ptprj*^{fl/fl} Col1a2^{Cre-ER(T)+/0} mice or Col1a2^{Cre-ER(T)+/0} (control) mice to BLM followed by administration of SDC2-pep beginning on day 10 after BLM, once daily, for 5 consecutive days. The SDC2-pep significantly inhibited pulmonary fibrosis in control mice, while in *Ptprj*^{fl/fl} Col1a2^{Cre-ER(T)+/0} mice the antifibrotic effect was significantly reduced but not absent (Figure 5, A-C, and Figure E9A), suggesting CD148-independent effects in lung fibroblasts or other cells in the fibrotic niche. SDC2-pep inhibited profibrotic gene expression (*Fn, Col1A1, Ctgf)* in control mice (Figure 5, C-D). There was a trend towards decreased BAL total cell counts in control mice treated with SDC2-pep but not in *Ptprj*^{fl/fl} Col1a2^{Cre-ER(T)+/0} mice (Figure E9B) after BLM.

Next, fibroblasts were stimulated with TGF-β1 in the absence or presence of SDC2-pep. TGF-β1 treatment increased the expression of p-Akt, p-mTOR, p62, p-IKKα/β, and α-SMA in wild type fibroblasts (Figure 5E, and Figure E10). This effect was markedly abrogated by treatment with SDC2-pep. In contrast, the inhibitory effect of SDC2-pep on TGF-β1-dependent expression of these signaling proteins in *Ptprj*^{-/-} fibroblasts was reduced (Figure 5E, and Figure E10). Similarly, SDC2-pep inhibited TGF-β1-induced *Fn* and *Col1a1* gene expression (Figure 5F) and cell

contractility (Figure 5G) in wild type fibroblasts. SDC-2 partially inhibited these effects in *Ptprj*^{-/-} fibroblasts, which had markedly enhanced pro-fibrotic responses to TGF-β1 stimulation (Figure 2, G-I). As shown in Figure E11, SDC2-pep dose-dependently inhibited *Col1a1* gene expression in wild type fibroblasts and *Ptprj*^{-/-} fibroblasts, further highlighting potential off-target effects of SDC2-pep in lung fibroblasts.

SDC2-pep inhibits pulmonary fibrosis in human IPF fibroblasts and ex vivo precision cut lung slices (PCLS)

We next evaluated the therapeutic potential of SDC2-pep in human IPF fibroblasts. Treatment with SDC2-pep significantly inhibited the activation of the PI3K/Akt/mTOR pathway in human IPF fibroblasts (Figure 6A, and Figure E12). SDC2-pep significantly inhibited the expression of p-Akt and p-mTOR in human IPF fibroblasts in scr-transfected but not in shCD148-transfected cells (Figure E10). SDC2-pep restored autophagy in human IPF fibroblasts in a CD148-dependent manner, as evidenced by increased relative LC3B-II expression and reduced p62 expression (Figure E12). SDC2-pep also inhibited ECM gene expression (*Fn, Col1a1*) (Figure 6A) and cell contractility (Figure 6B) and these effects were reduced in the absence of CD148. Furthermore, SDC2-pep significantly enhanced FasL-induced cell death in IPF fibroblasts and to a lesser extent in CD148-deficient cells (Figure 6D).

Finally, we tested the potential anti-fibrotic effect of SDC2-pep in precision cut lung slices (PCLS) derived from IPF lung explants obtained at the time of transplant. We exposed PCLS from IPF patients to SDC2-pep, which resulted in significantly decreased profibrotic gene expression (*Col1a1*, *Fn, Acta2*) in scr-transfected PCLS and this effect was reduced in shCD148-transfected PCLS (Figure 7 A-B). Flow cytometry in both fibroblasts and epithelial cells isolated from PCLS indicated that shCD148 reduced gene expression by approximately 60% (Figure E13 and E14). SDC2-pep did not affect *Ptprj* gene expression in PCLS (Figure 7C). Whereas shCD148 transfection of PCLS resulted in increased pro-fibrotic responses (Figure 7 A, B). Conversely, lentiviral overexpression of CD148 in PCLS from IPF lungs inhibited profibrotic gene expression

(*Col1a1*, *Fn, Acta2*) (Figure 7D). Finally, PCLS from control lungs were stimulated with a profibrotic mix in the presence or absence of SDC2-pep. SDC2-pep attenuated ECM gene expression (*Col1a1*, *Fn, Acta2*) but not *Ptprj* expression in response to stimulation with a profibrotic mix in control PCLS. SDC-2 pep also partially inhibited ECM expression in CD148 deficient PCLS, which had markedly increased pro-fibrotic responses to profibrotic mix (Figure 7, E-H). Taken together, our findings demonstrate that SDC2-pep inhibits lung fibrosis in human and experimental models of IPF predominantly through CD148, although CD148-independent effects may also contribute to its observed therapeutic effects. Our findings represent a new paradigm for the role of CD148 as a therapeutic target in IPF (Figure 8).

Discussion

Here, we demonstrate that protein tyrosine phosphatase-eta (PTPRJ/CD148) regulates profibrotic responses and lung fibroblast activation in IPF. Importantly, we show that CD148 is downregulated in clinical samples of IPF lung which in turn modulates profibrotic responses. In the current study, we use a conditional mouse approach to delineate the fibroblast-specific role of the receptor CD148 in mediating its anti-fibrotic effects in fibroblasts. We uncover a heretofore unknown role of NF-$\square$B in fibrogenesis and ECM regulation, and as a novel downstream pathway of CD148 signaling. We also uncover a novel effector pathway by which PI3K/Akt dependent modulation of autophagy *via* mTORC1 activation leads to aberrant p62 accumulation, which contributes to downstream NF-$\square$B activation. Additionally, we introduce a novel approach to therapeutic development in IPF, using a synthetic 18 amino-acid peptide derived from the SDC2 ectodomain. Since peptide-based approaches have been successfully developed for treatment of diverse medical conditions (37), our current study demonstrates that a SDC2-based peptide mimetic is a potential innovative therapy for IPF.

CD148 was previously reported as a regulator of T-cell, B-cell, macrophage and neutrophil function (38, 39). We demonstrate that CD148 downregulation in IPF fibroblasts contributes to cell activation, excessive ECM production and resistance to apoptosis. In a mouse model of

pulmonary fibrosis, targeted CD148 deficiency in fibroblasts exacerbates lung fibrosis by hyperactivation of PI3K/Akt/mTOR signaling, resulting in decreased autophagy. We have uncovered a novel mechanism by which impaired autophagy, *via* p62 accumulation, regulates NF-κB-dependent profibrotic responses in IPF lungs. Finally, we demonstrate that SDC2-pep, a CD148 agonist, can attenuate fibrosis in *in vitro*, *in vivo* and *ex vivo* models of pulmonary fibrosis through CD148-dependent mechanisms by regulating PI3K/Akt/mTOR signaling, restoring autophagy, and downregulating ECM gene expression. Remarkably, the SDC2 mimetic peptide provides a robust anti-fibrotic effect in IPF fibroblasts, despite a 50% reduction in CD148 expression in IPF lung tissue (Fig. 1 E-G).

Although nintedanib, one of the two FDA-approved drugs to treat IPF, is a known protein tyrosine kinase (PTK) inhibitor, the role of endogenous PTK inhibitors (i.e., protein tyrosine phosphatases, PTPs) in IPF remains incompletely understood. Prior studies investigating the regulation of cellular PTPs reveal divergent outcomes in experimental fibrosis with both potent pro- and antifibrotic effects reported (31, 40, 41). This may reflect the varying specificity of PTPs to dephosphorylate tyrosine residues, and differential subcellular localization and substrate specificities for signaling proteins (10). Furthermore, the majority of PTPs are expressed in different cell types, including immune cells, which may affect immune response or immune cell activation. Despite evidence implicating phosphatases in fibrogenesis, few investigative studies have developed effective therapies targeting phosphatase activity (42). We report here that an 18-aa SDC2-pep which activates CD148 potently inhibits fibroblast activation and attenuates pulmonary fibrosis. The antifibrotic effect of SDC2-pep was largely attenuated but not abolished in fibroblast-specific CD148 deficient mice, suggesting off-target effects in lung fibroblasts or regulation of additional receptor-mediated pathways in other cell types (e.g., alveolar epithelial cells) may mediate the therapeutic effects of SDC2-pep (17).

Autophagy is a cellular homeostatic process regulating the turnover of cellular organelles (i.e., mitochondria) and long-lived proteins. While considered a pro-survival response, autophagy plays

context-dependent roles in human disease progression (42). In IPF, low autophagy activity in fibroblasts may contribute to their profibrotic phenotype (43, 44). Here, we demonstrated that CD148 regulates autophagy *via* PI3K/Akt/mTOR signaling. However, CD148 deficiency also increases ECM gene expression *via* PI3K/Akt/mTOR signaling, suggesting transcriptional regulation of profibrotic gene expression. PI3K/Akt and mTOR activation may inhibit autophagy in activated fibroblasts. Thus, inhibition of the PI3K/Akt signaling pathway restores autophagy and inhibits fibrosis (30, 43). While low autophagy is associated with a profibrotic phenotype, the underlying mechanisms remain unclear. Rangarajan *et al.* demonstrated that autophagy regulates ECM production by removing excessive cytosolic collagen *via* autophagosomal degradation. Thus, the activation of autophagy by AMP-activated protein kinase (AMPK) activators (i.e*.,* metformin or 5-aminoimidazole-4-carboxamide riboside (AICAR)) inhibited excessive collagen expression *via* autophagosomal degradation (45). Interestingly, AMPK activators also inhibited ECM gene expression, not directly attributed to autophagosomal degradation. Hence, we hypothesized that autophagy may regulate transcriptional responses through distinct mechanisms. We demonstrate that low autophagy results in upregulation of profibrotic gene expression by enabling p62 accumulation, which is inversely correlated with autophagy activity (46). p62/SQSTM1 (sequestosome 1, ZIP3) contains multiple major domains such as PB1 and ZZ that confer the ability to interact with key components involved in essential signaling pathways. Importantly, p62 can regulate NF-κB *via* activation of IKK (46), which may contribute to cell survival, ECM production and myofibroblast transformation (47).

Our studies have uncovered a distinct role for NF-κB in profibrotic responses, which is of broad significance, since NF-κB transcriptional regulation is commonly associated with inflammatory, not fibroproliferative responses. We found that CD148 deficiency resulted in NF-κB hyperactivation which was required for enhanced ECM production in IPF fibroblasts. The hyperactivation of NF-κB by impaired autophagy provides a novel mechanistic link not previously

characterized for IPF and experimental fibrosis. Consistently, the ECM protein fibronectin (*Fn*) is tightly regulated by NF-κB, although there are no binding sites for NF-κB evident in the *Col1a1* and *Acta2* promoter regions (48, 49). Nevertheless, we found that CD148-deficient cells overexpress Col1a1 and αSMA and this effect was attenuated by an NF-κB inhibitor. NF-κB may possibly regulate ECM genes by indirect mechanisms, such that its subunits may interact with other transcription factors and regulate their transcriptional activity. For example, the p65 and p50 subunits of NF-κB can regulate the transcriptional activity of serum response factor and activator protein-1, which are implicated in *Acta2* and *Col1a1* gene expression, respectively (50, 51). NF-κB has also been shown to regulate the expression of multiple cytokines and chemokines now grouped as the senescence-associated secretory phenotype (SASP) factors (*e.g.,* IL-8, IL-6 and MCP-1) (52), which are associated with age-dependent organ fibrosis. Thus, further studies are needed to determine whether CD148 modulates cell senescence in fibrosis through regulation of p62/NF-κB signaling.

Our findings highlight CD148 as a key regulator of profibrotic responses in pulmonary fibroblasts. However, our data also suggest that CD148 is also downregulated in AT1 and AT2 cells from IPF lungs compared to control lungs. Interestingly, CD148 may regulate epithelial tight junctions by dephosphorylating tight junction proteins such as ZO-1 and occludin (53). Given that lung epithelial cell injury, integrity and hyperplasia represent hallmarks of lung fibrogenesis (1), future studies using conditional knockout approaches may elucidate new roles for CD148 in regulating lung epithelial cell responses to alveolar injury. Since immune cells may also contribute to fibrogenesis, the functional role of CD148 in immune cells also warrants investigation in fibrosis. Although we have identified a critical role of CD148 in fibroblast activation in pulmonary fibrosis and its underlying signaling processes, including novel roles for autophagy and NF-κB-dependent signaling, this work has several other limitations. First, the precise mechanisms and key intermolecular interactions by which NF-κB regulates profibrotic genes remain incompletely

elucidated, and further investigation will be needed. Second, the therapeutic effects of SDC-pep are not limited to CD148-dependent effects in fibroblasts, as SDC2 may have targeted effects in other fibroblast receptor or cell types, including epithelial cells in the fibrotic niche, which may account for partial therapeutic effects observed in fibroblast-specific *Ptprj*^{-/-} mice. Additional studies are required to elucidate specific secondary targets of the SDC2-pep. Finally, analysis of archival scRNAseq data (29) did not fully recapitulate the downregulation of myofibroblast CD148 observed in the current study. However, the differences between myofibroblast and fibroblast CD148 expression are intriguing and may further support the notion that CD148 regulates fibroblast/myofibroblast phenotypes in health and disease. Further translational studies using lungs obtained from independent cohorts and at various stages of disease progression will be needed to confirm the anti-fibrotic effects of CD148 and the efficacy of its therapeutic ligands. In conclusion, our findings highlight CD148 as a novel and promising avenue for therapeutic targeting in IPF.

References

1. Martinez FJ, Collard HR, Pardo A, Raghu G, Richeldi L, Selman M, Swigris JJ, Taniguchi H, Wells AU. Idiopathic pulmonary fibrosis. *Nat Rev Dis Primers* 2017; 3: 17074.

2. Chambers RC, Mercer PF. Mechanisms of alveolar epithelial injury, repair, and fibrosis. *Ann Am Thorac Soc* 2015; 12 Suppl 1: S16-20.

3. Richeldi L, du Bois RM, Raghu G, Azuma A, Brown KK, Costabel U, Cottin V, Flaherty KR, Hansell DM, Inoue Y, Kim DS, Kolb M, Nicholson AG, Noble PW, Selman M, Taniguchi H, Brun M, Le Maulf F, Girard M, Stowasser S, Schlenker-Herceg R, Disse B, Collard HR, Investigators IT. Efficacy and safety of nintedanib in idiopathic pulmonary fibrosis. *N Engl J Med* 2014; 370: 2071-2082.

4. Richeldi L, Costabel U, Selman M, Kim DS, Hansell DM, Nicholson AG, Brown KK, Flaherty KR, Noble PW, Raghu G, Brun M, Gupta A, Juhel N, Kluglich M, du Bois RM. Efficacy of a tyrosine kinase inhibitor in idiopathic pulmonary fibrosis. *N Engl J Med* 2011; 365: 1079-1087.

5. Harrod TR, Justement LB. Evaluating function of transmembrane protein tyrosine phosphatase CD148 in lymphocyte biology. *Immunol Res* 2002; 26: 153-166.

6. Gaya A, Pirotto F, Palou E, Autschbach F, Del Pozo V, Sole J, Serra-Pages C. CD148, a new membrane tyrosine phosphatase involved in leukocyte function. *Leuk Lymphoma* 1999; 35: 237-243.

7. Fournier P, Dussault S, Fusco A, Rivard A, Royal I. Tyrosine Phosphatase PTPRJ/DEP-1 Is an Essential Promoter of Vascular Permeability, Angiogenesis, and Tumor Progression. *Cancer Res* 2016; 76: 5080-5091.

8. Iuliano R, Trapasso F, Le Pera I, Schepis F, Sama I, Clodomiro A, Dumon KR, Santoro M, Chiariotti L, Viglietto G, Fusco A. An adenovirus carrying the rat protein tyrosine phosphatase eta suppresses the growth of human thyroid carcinoma cell lines in vitro and in vivo. *Cancer Res* 2003; 63: 882-886.

9. Kellie S, Craggs G, Bird IN, Jones GE. The tyrosine phosphatase DEP-1 induces cytoskeletal rearrangements, aberrant cell-substratum interactions and a reduction in cell proliferation. *J Cell Sci* 2004; 117: 609-618.

10. Julien SG, Dube N, Hardy S, Tremblay ML. Inside the human cancer tyrosine phosphatome. *Nat Rev Cancer* 2011; 11: 35-49.

11. Tsuboi N, Utsunomiya T, Roberts RL, Ito H, Takahashi K, Noda M, Takahashi T. The tyrosine phosphatase CD148 interacts with the p85 regulatory subunit of phosphoinositide 3-kinase. *Biochem J* 2008; 413: 193-200.

12. Omerovic J, Clague MJ, Prior IA. Phosphatome profiling reveals PTPN2, PTPRJ and PTEN as potent negative regulators of PKB/Akt activation in Ras-mutated cancer cells. *Biochem J* 2010; 426: 65-72.

13. Kral JB, Kuttke M, Schrottmaier WC, Birnecker B, Warszawska J, Wernig C, Paar H, Salzmann M, Sahin E, Brunner JS, Osterreicher C, Knapp S, Assinger A, Schabbauer G. Sustained PI3K Activation exacerbates BLM-induced Lung Fibrosis via activation of pro-inflammatory and pro-fibrotic pathways. *Sci Rep* 2016; 6: 23034.

14. Wygrecka M, Zakrzewicz D, Taborski B, Didiasova M, Kwapiszewska G, Preissner KT, Markart P. TGF-beta1 induces tissue factor expression in human lung

fibroblasts in a PI3K/JNK/Akt-dependent and AP-1-dependent manner. *Am J Respir Cell Mol Biol* 2012; 47: 614-627.

15. White ES, Thannickal VJ, Carskadon SL, Dickie EG, Livant DL, Markwart S, Toews GB, Arenberg DA. Integrin alpha4beta1 regulates migration across basement membranes by lung fibroblasts: a role for phosphatase and tensin homologue deleted on chromosome 10. *Am J Respir Crit Care Med* 2003; 168: 436-442.

16. Bartlett AH, Hayashida K, Park PW. Molecular and cellular mechanisms of syndecans in tissue injury and inflammation. *Mol Cells* 2007; 24: 153-166.

17. Shi Y, Gochuico BR, Yu G, Tang X, Osorio JC, Fernandez IE, Risquez CF, Patel AS, Shi Y, Wathelet MG, Goodwin AJ, Haspel JA, Ryter SW, Billings EM, Kaminski N, Morse D, Rosas IO. Syndecan-2 exerts antifibrotic effects by promoting caveolin-1-mediated transforming growth factor-beta receptor I internalization and inhibiting transforming growth factor-beta1 signaling. *Am J Respir Crit Care Med* 2013; 188: 831-841.

18. Tsoyi K, Chu SG, Patino-Jaramillo NG, Wilder J, Villalba J, Doyle-Eisele M, McDonald J, Liu X, El-Chemaly S, Perrella MA, Rosas IO. Syndecan-2 Attenuates Radiation-induced Pulmonary Fibrosis and Inhibits Fibroblast Activation by Regulating PI3K/Akt/ROCK Pathway via CD148. *Am J Respir Cell Mol Biol* 2018; 58: 208-215.

19. De Rossi G, Evans AR, Kay E, Woodfin A, McKay TR, Nourshargh S, Whiteford JR. Shed syndecan-2 inhibits angiogenesis. *J Cell Sci* 2014; 127: 4788-4799.

20. Whiteford JR, Xian X, Chaussade C, Vanhaesebroeck B, Nourshargh S, Couchman JR. Syndecan-2 is a novel ligand for the protein tyrosine phosphatase receptor CD148. *Mol Biol Cell* 2011; 22: 3609-3624.

21. Tsoyi K, Chu S, Xiong K, Ith B, Exposito A, Poli S, Ayaub E, Liu X, El-Chemaly, Perrella M, Rosas IO. Receptor type protein tyrosine phosphatase η (PTPRJ/CD148) deficiency in fibroblasts leads to increased fibrosis by regulating PI3K/Akt/mTOR signaling, autophagy and p62 Level. *Am J Respir Crit Care Med.* 2020, 201:A1235.

22. Tsoyi K, Hall SR, Dalli J, Colas RA, Ghanta S, Ith B, Coronata A, Fredenburgh LE, Baron RM, Choi AM, Serhan CN, Liu X, Perrella MA. Carbon Monoxide Improves Efficacy of Mesenchymal Stromal Cells During Sepsis by Production of Specialized Proresolving Lipid Mediators. *Crit Care Med* 2016; 44: e1236-e1245.

23. Adolph TE, Tomczak MF, Niederreiter L, Ko HJ, Bock J, Martinez-Naves E, Glickman JN, Tschurtschenthaler M, Hartwig J, Hosomi S, Flak MB, Cusick JL, Kohno K, Iwawaki T, Billmann-Born S, Raine T, Bharti R, Lucius R, Kweon MN, Marciniak SJ, Choi A, Hagen SJ, Schreiber S, Rosenstiel P, Kaser A, Blumberg RS. Paneth cells as a site of origin for intestinal inflammation. *Nature* 2013; 503: 272-276.

24. Uhl FE, Vierkotten S, Wagner DE, Burgstaller G, Costa R, Koch I, Lindner M, Meiners S, Eickelberg O, Konigshoff M. Preclinical validation and imaging of Wnt-induced repair in human 3D lung tissue cultures. *Eur Respir J* 2015; 46: 1150-1166.

25. Bai Y, Krishnamoorthy N, Patel KR, Rosas I, Sanderson MJ, Ai X. Cryopreserved Human Precision-Cut Lung Slices as a Bioassay for Live Tissue Banking. A Viability Study of Bronchodilation with Bitter-Taste Receptor Agonists. *Am J Respir Cell Mol Biol* 2016; 54: 656-663.

26. Tsoyi K, Kim HJ, Shin JS, Kim DH, Cho HJ, Lee SS, Ahn SK, Yun-Choi HS, Lee JH, Seo HG, Chang KC. HO-1 and JAK-2/STAT-1 signals are involved in preferential inhibition of iNOS over COX-2 gene expression by newly synthesized tetrahydroisoquinoline alkaloid, CKD712, in cells activated with lipopolysacchride. *Cell Signal* 2008; 20: 1839-1847.

27. Schmittgen TD, Livak KJ. Analyzing real-time PCR data by the comparative C(T) method. *Nat Protoc* 2008; 3: 1101-1108.

28. Fujino N, Kubo H, Ota C, Suzuki T, Suzuki S, Yamada M, Takahashi T, He M, Suzuki T, Kondo T, Yamaya M. A novel method for isolating individual cellular components from the adult human distal lung. *Am J Respir Cell Mol Biol* 2012; 46: 422-430.

29. Adams TS, Schupp JC, Poli S, Ayaub EA, Neumark N, Ahangari F, Chu SG, Raby BA, DeIuliis G, Januszyk M, Duan Q, Arnett HA, Siddiqui A, Washko GR, Homer R, Yan X, Rosas IO, Kaminski N. Single-cell RNA-seq reveals ectopic and aberrant lung-resident cell populations in idiopathic pulmonary fibrosis. *Sci. Adv.* 2020; 6(28): eaba1983.

30. Romero Y, Bueno M, Ramirez R, Alvarez D, Sembrat JC, Goncharova EA, Rojas M, Selman M, Mora AL, Pardo A. mTORC1 activation decreases autophagy in aging

and idiopathic pulmonary fibrosis and contributes to apoptosis resistance in IPF fibroblasts. *Aging Cell* 2016; 15: 1103-1112.

31. Bamberg A, Redente EF, Groshong SD, Tuder RM, Cool CD, Keith RC, Edelman BL, Black BP, Cosgrove GP, Wynes MW, Curran-Everett D, De Langhe S, Ortiz LA, Thorburn A, Riches DWH. Protein Tyrosine Phosphatase-N13 Promotes Myofibroblast Resistance to Apoptosis in Idiopathic Pulmonary Fibrosis. *Am J Respir Crit Care Med* 2018; 198: 914-927.

32. Nho RS, Peterson M, Hergert P, Henke CA. FoxO3a (Forkhead Box O3a) deficiency protects Idiopathic Pulmonary Fibrosis (IPF) fibroblasts from type I polymerized collagen matrix-induced apoptosis via caveolin-1 (cav-1) and Fas. *PLoS One* 2013; 8: e61017.

33. Nho RS, Hergert P. IPF fibroblasts are desensitized to type I collagen matrix-induced cell death by suppressing low autophagy via aberrant Akt/mTOR kinases. *PLoS One* 2014; 9: e94616.

34. Duran A, Linares JF, Galvez AS, Wikenheiser K, Flores JM, Diaz-Meco MT, Moscat J. The signaling adaptor p62 is an important NF-kappaB mediator in tumorigenesis. *Cancer Cell* 2008; 13: 343-354.

35. Moscat J, Diaz-Meco MT. p62: a versatile multitasker takes on cancer. *Trends Biochem Sci* 2012; 37: 230-236.

36. Takahashi K, Mernaugh RL, Friedman DB, Weller R, Tsuboi N, Yamashita H, Quaranta V, Takahashi T. Thrombospondin-1 acts as a ligand for CD148 tyrosine phosphatase. *Proc Natl Acad Sci U S A* 2012; 109: 1985-1990.

37. Fosgerau K, Hoffmann T. Peptide therapeutics: current status and future directions. *Drug Discov Today* 2015; 20: 122-128.

38. Zhu JW, Doan K, Park J, Chau AH, Zhang H, Lowell CA, Weiss A. Receptor-like tyrosine phosphatases CD45 and CD148 have distinct functions in chemoattractant-mediated neutrophil migration and response to S. aureus. *Immunity* 2011; 35: 757-769.

39. Skrzypczynska KM, Zhu JW, Weiss A. Positive Regulation of Lyn Kinase by CD148 Is Required for B Cell Receptor Signaling in B1 but Not B2 B Cells. *Immunity* 2016; 45: 1232-1244.

40. Aschner Y, Khalifah AP, Briones N, Yamashita C, Dolgonos L, Young SK, Campbell MN, Riches DW, Redente EF, Janssen WJ, Henson PM, Sap J, Vacaresse N, Kapus A, McCulloch CA, Zemans RL, Downey GP. Protein tyrosine phosphatase alpha mediates profibrotic signaling in lung fibroblasts through TGF-beta responsiveness. *Am J Pathol* 2014; 184: 1489-1502.

41. Tzouvelekis A, Yu G, Lino Cardenas CL, Herazo-Maya JD, Wang R, Woolard T, Zhang Y, Sakamoto K, Lee H, Yi JS, DeIuliis G, Xylourgidis N, Ahangari F, Lee PJ, Aidinis V, Herzog EL, Homer R, Bennett AM, Kaminski N. SH2 Domain-Containing Phosphatase-2 Is a Novel Antifibrotic Regulator in Pulmonary Fibrosis. *Am J Respir Crit Care Med* 2017; 195: 500-514.

42. Lazo JS, Sharlow ER. Drugging Undruggable Molecular Cancer Targets. *Annu Rev Pharmacol Toxicol* 2016; 56: 23-40.

43. Patel AS, Lin L, Geyer A, Haspel JA, An CH, Cao J, Rosas IO, Morse D. Autophagy in idiopathic pulmonary fibrosis. *PLoS One* 2012; 7: e41394.

44. Bueno M, Lai YC, Romero Y, Brands J, St Croix CM, Kamga C, Corey C, Herazo-Maya JD, Sembrat J, Lee JS, Duncan SR, Rojas M, Shiva S, Chu CT, Mora AL. PINK1 deficiency impairs mitochondrial homeostasis and promotes lung fibrosis. *J Clin Invest* 2015; 125: 521-538.

45. Rangarajan S, Bone NB, Zmijewska AA, Jiang S, Park DW, Bernard K, Locy ML, Ravi S, Deshane J, Mannon RB, Abraham E, Darley-Usmar V, Thannickal VJ, Zmijewski JW. Metformin reverses established lung fibrosis in a bleomycin model. *Nat Med* 2018; 24: 1121-1127.

46. Puissant A, Fenouille N, Auberger P. When autophagy meets cancer through p62/SQSTM1. *Am J Cancer Res* 2012; 2: 397-413.

47. Mia MM, Bank RA. The IkappaB kinase inhibitor ACHP strongly attenuates TGFbeta1-induced myofibroblast formation and collagen synthesis. *J Cell Mol Med* 2015; 19: 2780-2792.

48. Buttner C, Skupin A, Rieber EP. Transcriptional activation of the type I collagen genes COL1A1 and COL1A2 in fibroblasts by interleukin-4: analysis of the functional collagen promoter sequences. *J Cell Physiol* 2004; 198: 248-258.

49. Shimizu RT, Blank RS, Jervis R, Lawrenz-Smith SC, Owens GK. The smooth muscle alpha-actin gene promoter is differentially regulated in smooth muscle versus non-smooth muscle cells. *J Biol Chem* 1995; 270: 7631-7643.

50. Franzoso G, Carlson L, Brown K, Daucher MB, Bressler P, Siebenlist U. Activation of the serum response factor by p65/NF-kappaB. *EMBO J* 1996; 15: 3403-3412.

51. Fujioka S, Niu J, Schmidt C, Sclabas GM, Peng B, Uwagawa T, Li Z, Evans DB, Abbruzzese JL, Chiao PJ. NF-kappaB and AP-1 connection: mechanism of NF-kappaB-dependent regulation of AP-1 activity. *Mol Cell Biol* 2004; 24: 7806-7819.

52. Salminen A, Kauppinen A, Kaarniranta K. Emerging role of NF-kappaB signaling in the induction of senescence-associated secretory phenotype (SASP). *Cell Signal* 2012; 24: 835-845.

53. Sallee JL, Burridge K. Density-enhanced phosphatase 1 regulates phosphorylation of tight junction proteins and enhances barrier function of epithelial cells. *J Biol Chem* 2009; 284: 14997-15006.
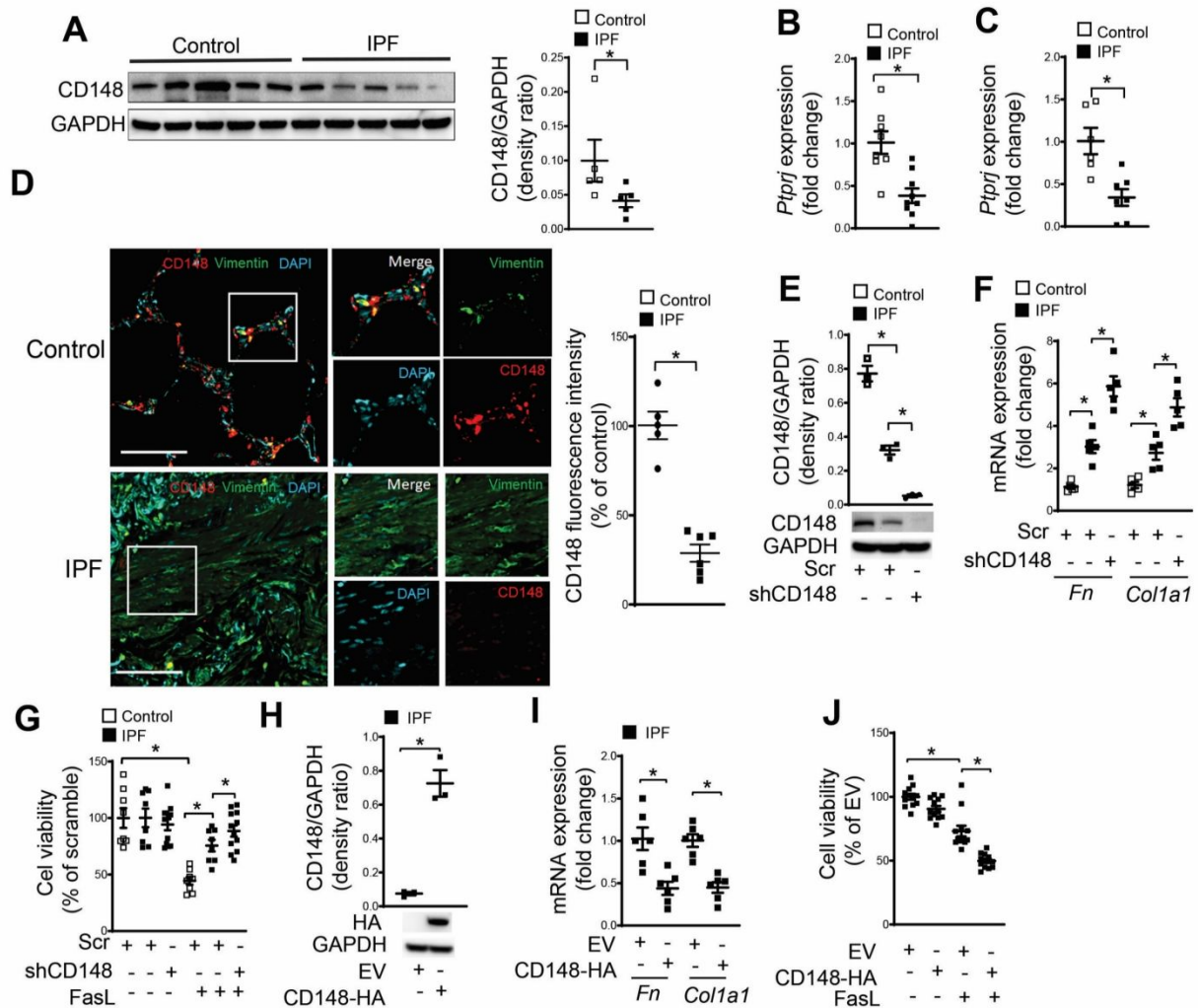
Fig. 1. CD148 is downregulated in IPF lung and contributes to pro-fibrotic phenotype of IPF-derived lung fibroblasts. (**A**) CD148 protein expression levels were determined in lung homogenates from control (*n*=5) and IPF (*n*=5) patients. (Graphic) Densitometry (by ImageJ software). (**B**) Lung specimens from control (*n*=9) and IPF (*n*=10) patients were homogenized and subjected to total RNA isolation. *Ptprj* (CD148) mRNA levels were assessed using qPCR. (**C**) Single cell suspensions of control (*n*=6) and IPF (*n*=7) were enriched for fibroblasts (see Fig. S1). mRNA expression of CD148 in fibroblast-enriched cell populations were assessed using qPCR. (**D**) Representative fluorescence microscopy images of CD148 (Cy3, red), Vimentin (GFP, green) and DAPI (blue) in control (*n*=4) and IPF lung tissue (*n*=5). Scale bar = 100 μm. Enlarged areas (Clockwise from top right panel) represent Vimentin, CD148, DAPI and merged

image. CD148 fluorescence intensity was quantified by ImageJ. (**E-F**) Lung fibroblasts from

non-disease (control) and IPF samples were transfected with scramble (Scr) or shCD148. (**E**)

CD148 protein levels were measured by western blot (*n*=3). (**F**) mRNA levels of fibronectin (*Fn*)

and Collagen 1a1 (*Col1a1*) were measured using qPCR (*n*=5). (**G**) Scr and shCD148

transfected cells were seeded in 24 well plates and then treated with Fas ligand (FasL, 200

ng/ml) for 24 h. After treatment, cell viability was determined using the MTT assay (*n*=5). (**H**)

IPF-derived lung fibroblasts were stably transfected with empty vector (EV, pLenti-GIII-HA) or

pLenti-GIII-CD148-HA (CD148-HA). The cells were lysed and subjected to western blot to

measure hemagglutinin tag (HA) (*n*=3). (**I**) In EV and CD148-HA transfected cells, the

expression of *Fn* and *Col1a1* were measured using qPCR (*n*=5). (**J**) EV and CD148-HA

transfected cells were seeded at equal amounts in 24 well plates and treated with FasL (200

ng/ml) for 24 h. Cell viability was determined using the MTT assay (*n*=5). Data are mean ±

s.e.m. *P<0.05, by Mann-Whitney's unpaired non-parametric test (E and H), Student's unpaired

t test (**B and C**), one-way ANOVA (**F, G, I, J**).
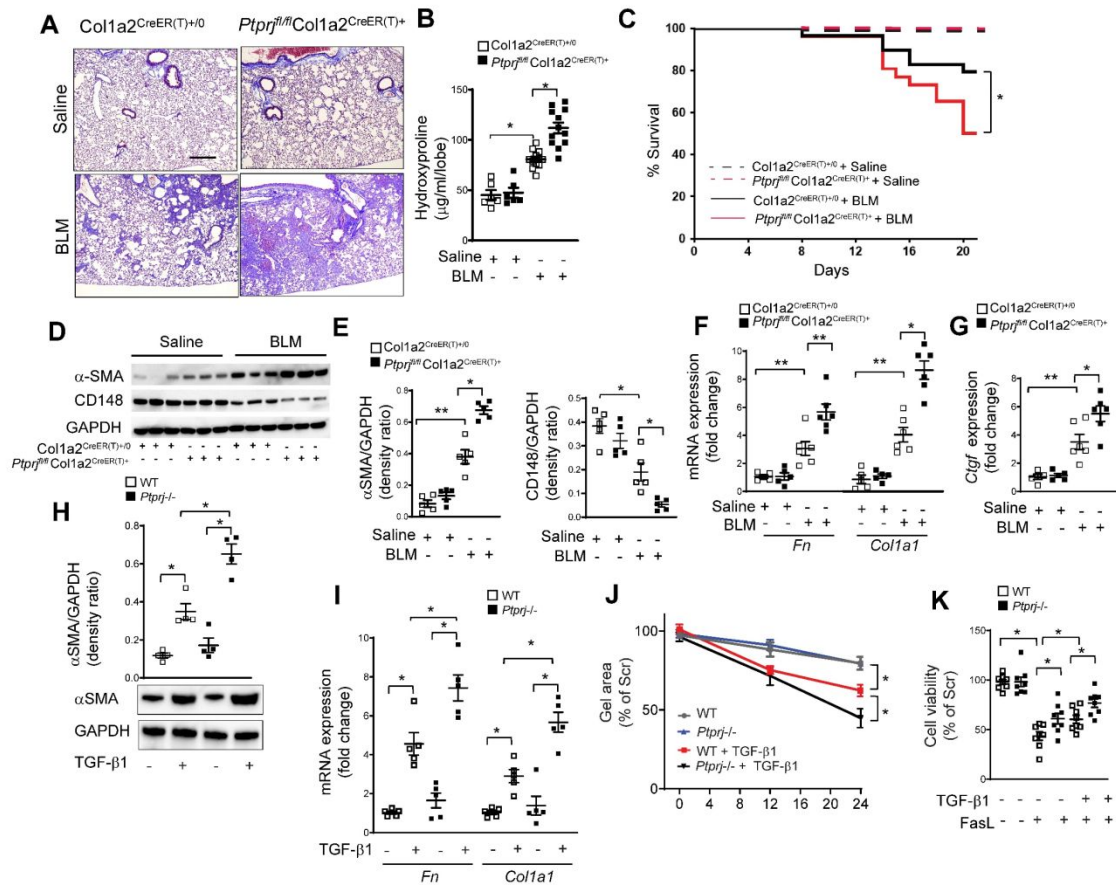
Fig. 2. CD148 deficiency in fibroblasts worsens pulmonary fibrosis in bleomycin-treated mice and increases fibroblast activation in response to TGF-β1. CD148 fibroblast-specific knockout mice (*Ptprj*^{fl/fl} Col1a2^{Cre-ER(T)+/0}) were developed as described in Methods. (**A**) *Ptprj*^{fl/fl} Col1a2^{Cre-ER(T)+/0} mice or Col1a2^{Cre-ER(T)+/0} (wild type) mice were exposed to BLM to induce lung fibrosis. At day 21, mouse lungs were harvested and stained with Masson's trichrome (*n*=3 for saline and *n*=5 for BLM groups). (**B**) Hydroxyproline content was measured in the left lung of *Ptprj*^{fl/fl} Col1a2^{Cre-ER(T)+/0} mice (*n*=12) and Col1a2^{Cre-ER(T)+/0} (WT) mice (*n*=12) exposed to BLM, and *Ptprj*^{fl/fl} Col1a2^{Cre-ER(T)+/0} (*n*=6) and Col1a2^{Cre-ER(T)+/0} (*n*=6) exposed to saline; at day 21. (**C**) Relative survival at day 0-21 after BLM. (**D-E**), α-SMA and CD148 expression in harvested lungs were measured by western blot (*n*=3-5 for each condition). (**F-G**) Gene expression of *Fn* and *Col1a1*,

and *Ctgf* in harvested lungs was measured using qPCR (*n*=5 for each condition). (**H-I**), Mouse lung fibroblasts from *Ptprj*$^{fl/fl}$ Col1a2$^{Cre-ER(T)+/0}$ mice (*Ptprj*$^{-/-}$) and Col1a2$^{Cre-ER(T)+/0}$ (WT) mice were isolated and treated with 4-OHT (1 μM) for 24 h. After 4-OHT treatment, cells were exposed to TGF-β1 (10 ng/ml) for an additional 24 h. After stimulation, cells were harvested. (**H**) western blot (*n*=4 for each condition). (**I**) mRNA levels of *Col1a1* and *Fn* were measured by qPCR (*n*=5 for each condition). (**J**) Cells were mixed with collagen 1. Gel contractility was measured at 0, 12 and 24 h after TGF-β1 (10 ng/ml) stimulation (*n*=6 for each condition). (**K**) Cell death was induced by FasL (200 ng/ml). At 24 h, cell viability was measured with MTT assay (*n*=5 for each condition). Data are mean ± s.e.m. *P<0.05, by one-way ANOVA.
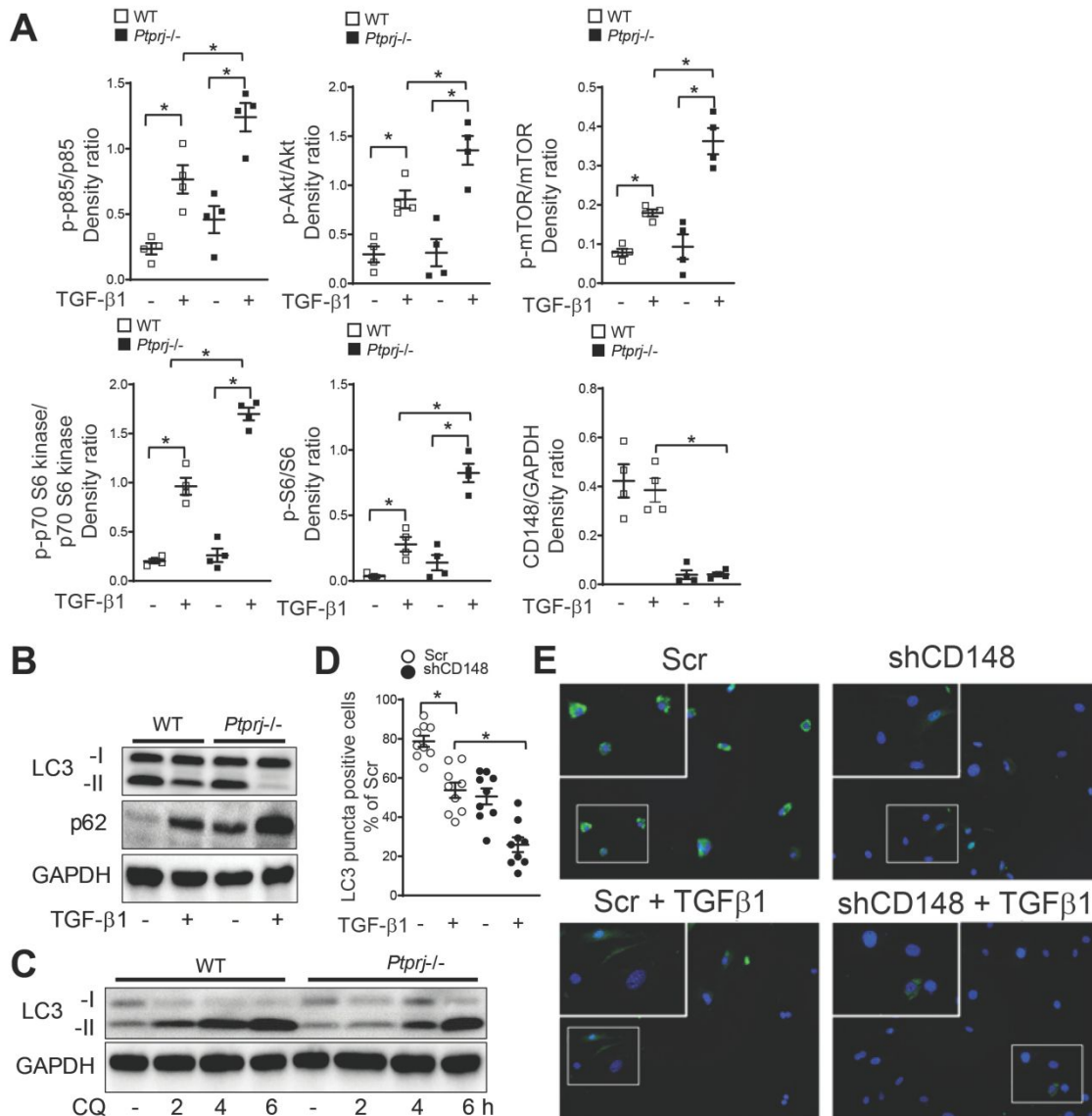
Fig. 3. CD148 deficiency enhances PI3K/Akt/mTOR signaling which results in low autophagy, high p62 expression in lung fibroblasts. (**A**) Mouse lung fibroblasts were isolated from *Ptprj*^{fl/fl} Col1a2[Cre-ER(T)+/0] mice (*Ptprj*^{-/-}) and Col1a2[Cre-ER(T)+/0] mice (WT) and then treated with 4-OHT (1 µM) for 24 h. After 4-OHT treatment, cells were exposed to TGF-β1 (10 ng/ml) for 24 h. After stimulation, cells were harvested, and the expression of p-p85 (Tyr458), p-Akt (Ser473), p-mTOR (Ser2448), p-p70 S6 kinase (Thr389), p-S6 ribosomal protein (Ser235/236) and CD148 (*n*=4 for each condition) in lysates was determined by Western immunoblotting and corresponding

densitometry (ImageJ software). Data were normalized to corresponding dephospho- forms or GAPDH. (**B**) WT and *Ptprj*^{-/-} cells were stimulated with TGF-β1 (10 ng/ml) for 24 h. Then cells were lysed and LC3-I and -II and p62 were measured by western blot (*n*=4). (**C**) WT and *Ptprj*^{-/-} cells were incubated in starvation media (Hank's buffered salt solution (HBSS, without calcium/magnesium) containing 1% regular medium) for 24 h. Then, autophagy flux was measured by LC3-II accumulation in the absence or presence of lysosomal acidification inhibitor chloroquine (25 µM) at 2, 4 and 6 h (*n*=4). (**D-E**) Lung fibroblasts from LC3-GFP transgenic mice were transfected with scr or shCD148 (lentivirus). Cells were starved for 24 h in the presence or absence of TGF-β1 (10 ng/ml), then cells were treated with chloroquine (25 µM) for 4 h. After treatment cells were fixed and digital images (3 images per sample) were taken using fluorescent microscope. Representative images are shown in (E). LC3 puncta positive cells were quantified using ImageJ (D). Data are mean ± s.e.m. *P*<0.05, by one-way ANOVA.
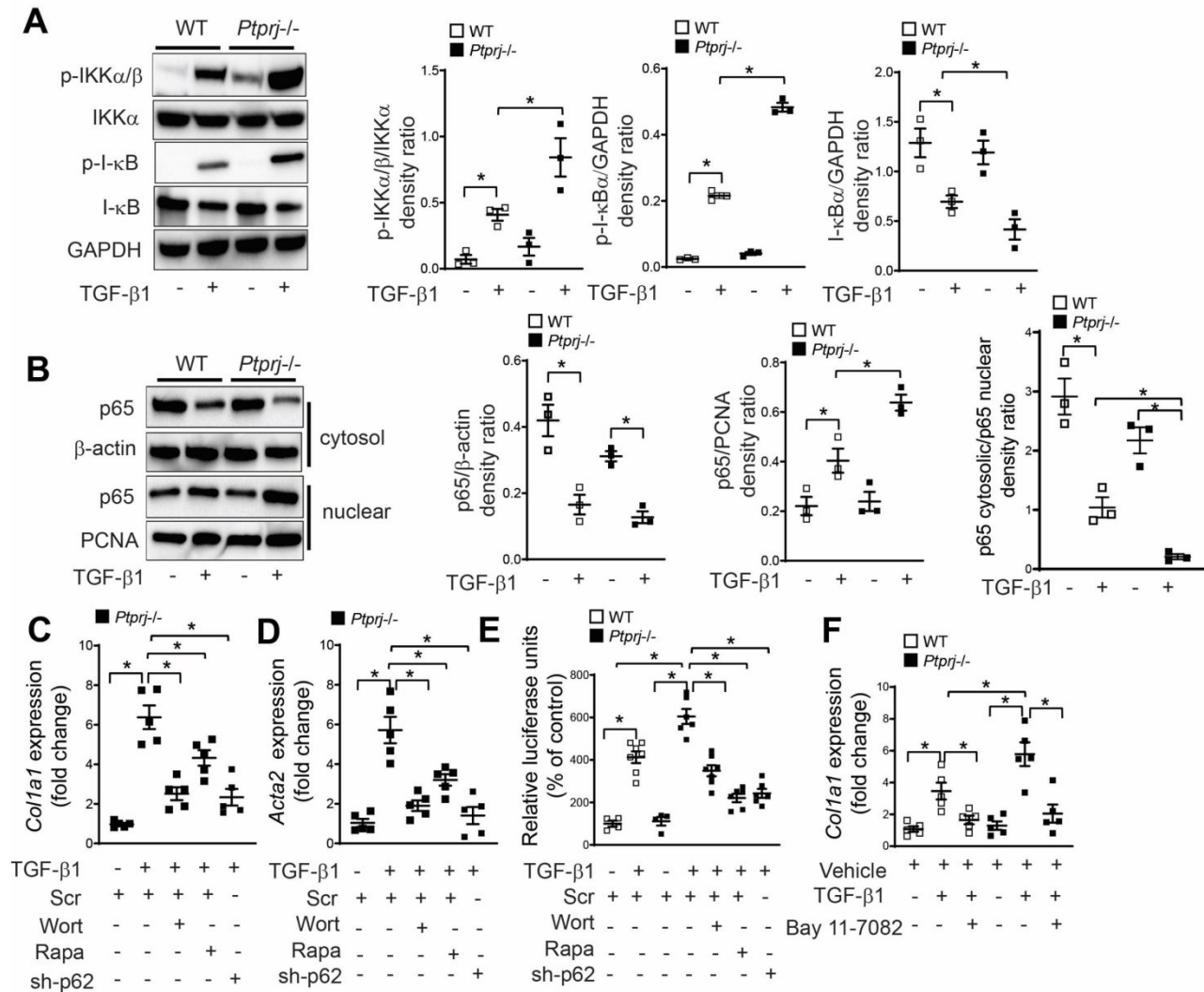
Fig. 4. CD148 deficiency enhances PI3K/Akt/mTOR signaling which results in enhanced NF-κB activation in lung fibroblasts. (**A**) WT and *Ptprj*^{-/-} cells were stimulated with TGF-β1 (10 ng/ml) for 24 h. Cells were lysed and p-IKKα/β, p-IκB and IκB were measured by western blot (*n*=4). GAPDH was the standard. Bar graphs at right are the quantitation of corresponding proteins. (**B**) WT and *Ptprj*^{-/-} cells were stimulated with TGF-β1 (10 ng/ml) for 24 h. Cells were subjected to cytosol and nuclear protein fractionation. The p65 (NF-κB subunit) nuclear translocation was measured by western blot (*n*=3). β-actin and PCNA were used as cytosolic and nuclear markers, respectively. Bar graphs at right are the quantitation of corresponding proteins.

p65 cytosolic/nuclear ratio is shown (*far right*). Data are mean ± s.e.m. *P<0.05, by Kurskal-Wallis non-parametric test (**C-D**) WT or *Ptprj*^{-/-} cells were transfected with scr or shp62 (lentivirus). Cells were stimulated with TGF-β1 (10 ng/ml) in the presence or absence or wortmannin (wort, 50 nM) or rapamycin (rapa, 1 µM). At 24 h cells were harvested and subjected to qPCR for *Col1a1* or *Acta2* (*n*=5). (**E**) WT or *Ptprj*^{-/-} cells were transfected with NF-κB luciferase reporter plasmid in the presence or absence of scr or shp62, or wort (50 nM) or rapa (1 µM). Then, cells were treated with TGF-β1 (10 ng/ml) for 4 h. Luciferase activity were measured as described in methods (*n*=4 or 7). Data are mean ± s.e.m. *P<0.05, by one-way ANOVA. (**F**) WT or *Ptprj*^{-/-} cells were stimulated with TGF-β1 (10 ng/ml) in the presence or absence of the NF-$\square$B inhibitor Bay 11-7082 (10 µM). mRNA levels of *Col1a1* were measured by qPCR (*n*=5 for each condition). Data are mean ± s.e.m. *P<0.05, by one-way ANOVA.
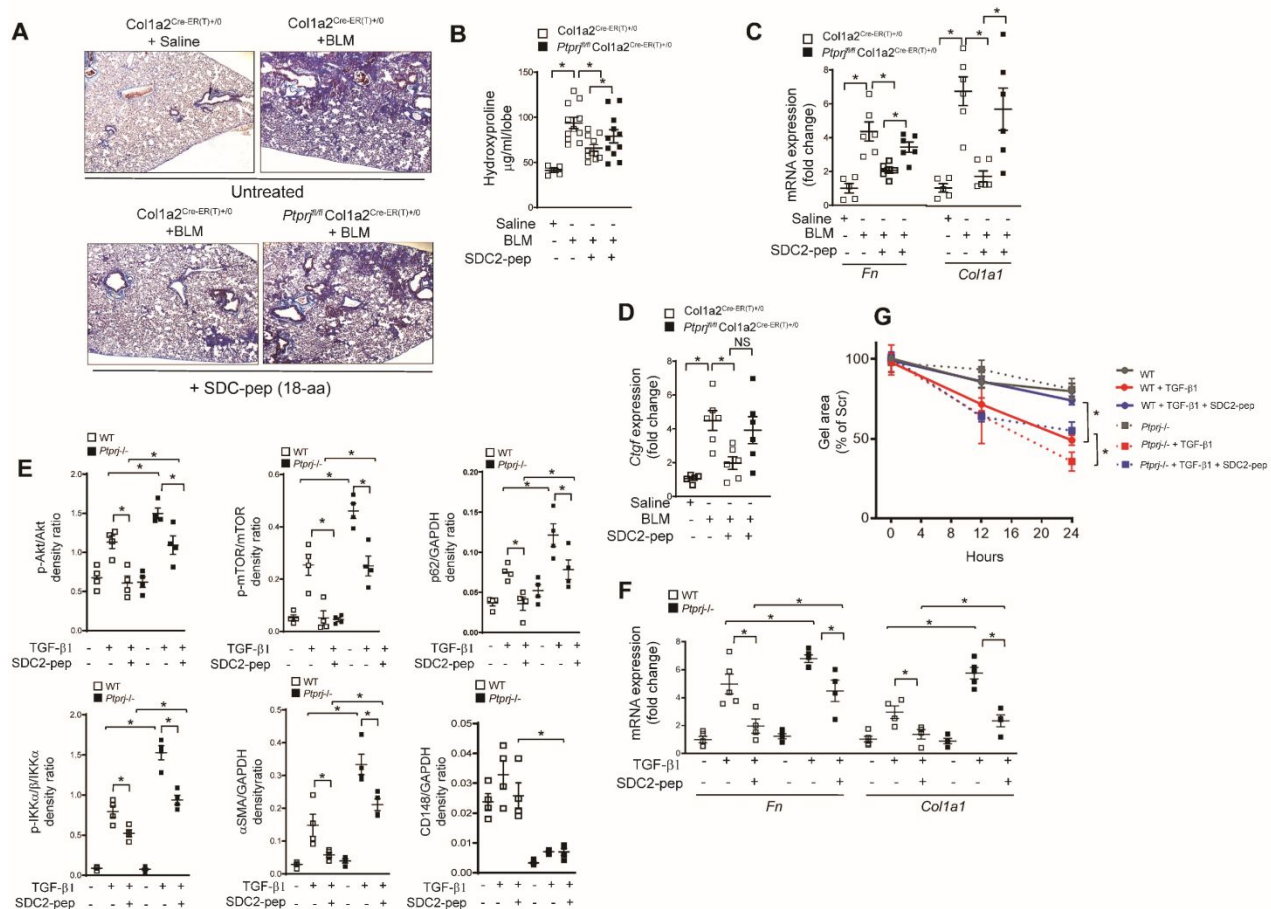
Fig. 5. SDC2 18-aa peptide inhibits pulmonary fibrosis *in vivo*; upregulates autophagy by downregulation of PI3K/Akt/mTOR signaling and inhibits ECM gene expression in mouse fibroblasts *via* CD148. (A-C) *Ptprj*^{fl/fl} Col1a2[Cre-ER(T)+/0] mice (fibroblast-specific CD148 deficient) and Col1a2[Cre-ER(T)+/0] (WT) mice were exposed to BLM. SDC2 18-aa peptide (SDC2-pep, 0.5 mg/kg) was intranasally delivered into WT and *Ptprj*^{fl/fl} Col1a2[Cre-ER(T)+/0] mice 10 days after BLM injury. Treatments were repeated at day 12, 14, 16 and 18. (**A**) At 24 days after BLM exposure lungs were harvested and stained with Masson's trichrome (*n*=3 for saline and *n*=5 for BLM groups). (**B**) Hydroxyproline content was measured in the left lung of mice exposed to BLM (*n*=11) or saline (*n*=5). Gene expression of (**C**) *Fn* and *Col1a1*; and (**D**) connective tissue growth factor (*Ctgf*) in harvested lungs were measured using qPCR (*n*=5 for each condition). (**E-F**) Mouse lung fibroblasts from *Ptprj*^{fl/fl} Col1a2[Cre-ER(T)+/0] mice (*Ptprj*^{-/-}) and Col1a2[Cre-ER(T)+/0] mice (WT) were

isolated and treated with 4-OHT (1 μM) for 24 h. After 4-OHT treatment, cells were exposed to ±TGF-β1 (10 ng/ml) for an additional 24 h, in the absence or presence of SDC2-pep (5 μM). (**E**) Expression of p-AKT/Akt, p-mTOR/mTOR, p62/GAPDH p-IKKα/β/IKKα, α-SMA/GAPDH, and CD148/GAPDH was determined by Western immunoblotting (*n*=4), and corresponding densitometry (ImageJ software). Data are mean ± s.e.m. *P<0.05, by one-way ANOVA. (**F**) mRNA levels of *Col1a1* and *Fn* were measured by qPCR (*n*=5 for each condition). (**G**) After treatment, cells were mixed with collagen 1. Gel contractility was measured at 0, 12, and 24 h after TGF-β1 stimulation (*n*=6 for each condition). Data are mean ± s.e.m. *P<0.05, by one-way ANOVA.
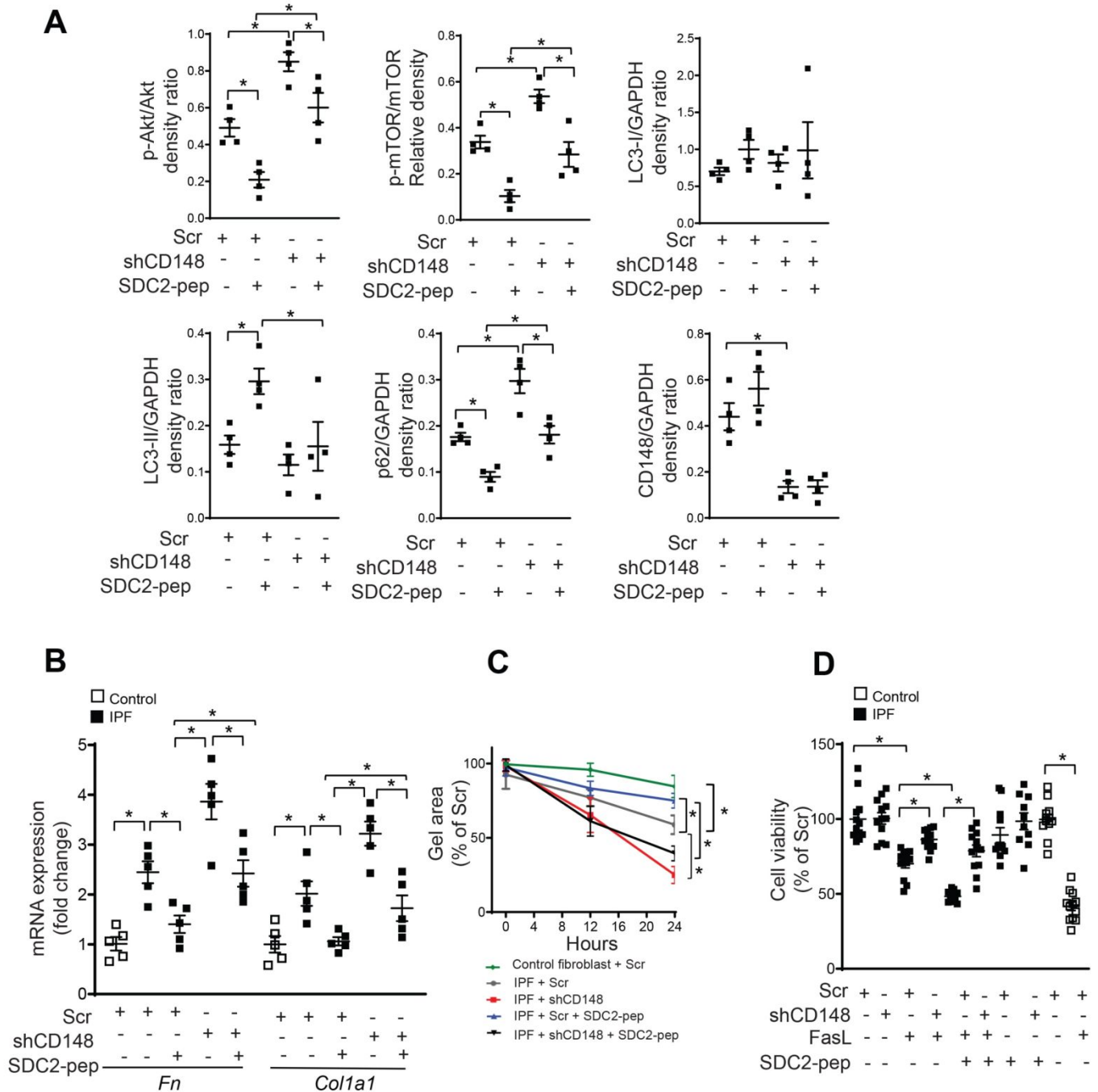
Fig. 6. SDC2 18-aa peptide attenuates pro-fibrotic gene expression in human IPF fibroblasts. (**A**) IPF-derived lung fibroblasts were transfected with scr or shCD148. Then cells were treated with SDC2 18-aa peptide (5 μM) for 24 h. After incubation, p-Akt (Ser473), p-mTOR (Ser2448), LC3, p62 and CD148 were measured by western blot (*n*=4). Band intensities were quantified using ImageJ software and were expressed as a ratio of band intensity relative to

GAPDH. Data are mean ± s.e.m. *P<0.05, by one-way ANOVA. (**B**) mRNA levels of *Fn* and *Col1a1* were measured by qPCR (*n*=5). (**C**) Scr or shCD148 transfected control or IPF-derived lung fibroblasts were mixed with collagen 1. Gel contractility were measured at 0, 12 and 24 h in the presence or absence of SDC2-pep (5 μM), *n*=5/group. (**D**) Scr or shCD148 transfected control or IPF-derived lung fibroblasts were treated with FasL (200 ng/ml) for 24 h in the presence or absence of SDC2-pep (5 μM) (*n*=7). Cell viability was measured using MTT assay. Data are mean ± s.e.m. *P<0.05, by one-way ANOVA.
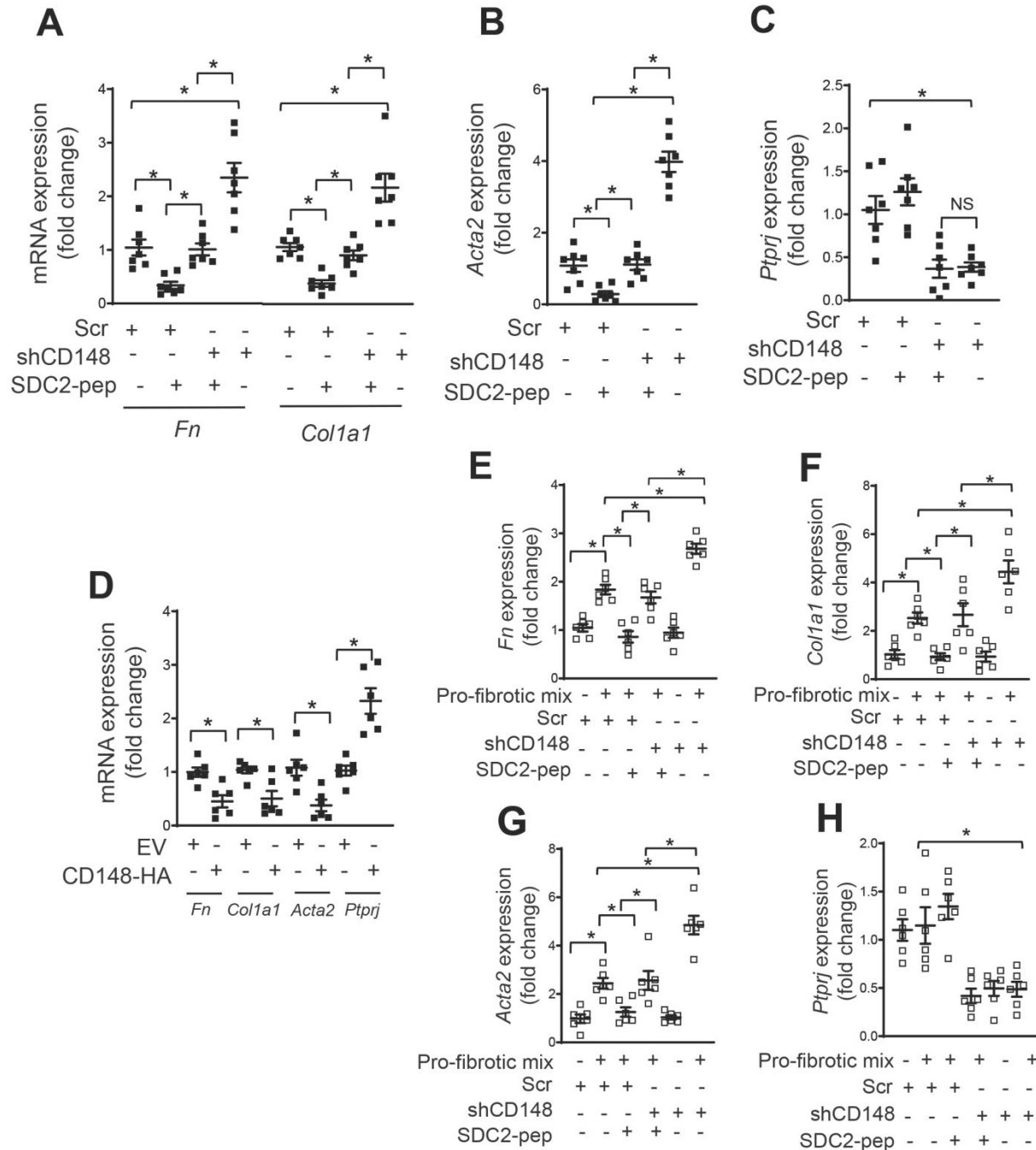
Fig. 7. SDC2 18-aa peptide and CD148 overexpression attenuate pro-fibrotic gene expression in PCLSs derived from IPF lungs, and from wild type lungs subjected to pro-fibrotic stimuli. (**A-D**) PCLS from IPF lungs were transfected with Scr, shCD148 or EV and CD148-HA. Then, PCLS were treated with SDC2-pep (5 μM) for 72 h. After incubation, PCLS were digested for total RNA isolation. The expression of (**A**) *Fn* and *Col1a1*, (**B**) *Acta2*, and (**C**)

Ptprj (CD148) were measured by qPCR (*n*=7 for each condition). (**D**) mRNA levels of *Col1a1*, *Fn*, *Acta2* and *Ptprj* (CD148) were measured by qPCR in EV and CD148 overexpressing PCLS (CD148-HA). (**E-H**) PCLS from control lungs were transfected with Scr, shCD148 (lentivirus). Then, PCLSs were treated with pro-fibrotic mix (FGF basic, 25 ng/ml, PDGF-BB, 10 ng/ml, TGF-β1, 10 ng/ml) 72 h with or without SDC2-pep (5 μM). After incubation, slices were digested for total RNA isolation. The expression of **E,** *Fn*, **F,** *Col1a1*, **G,** *Acta2*, and **H,** *Ptprj* were measured by qPCR. (A-H, *n*=6 for each condition). Data are mean ± s.e.m. *$P<0.05$, by one-way ANOVA.
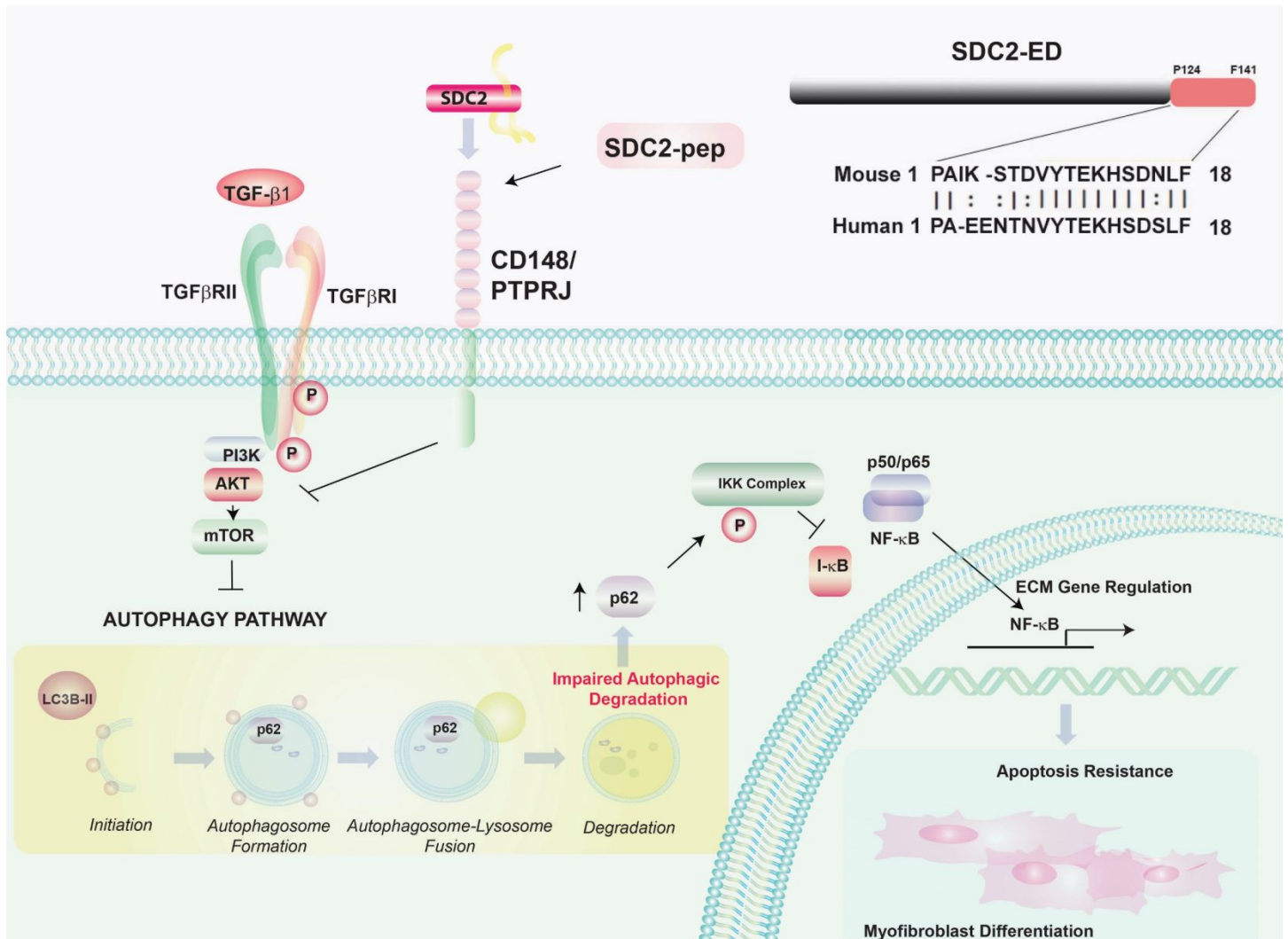
Fig. 8. Schema depicting proposed antifibrotic effects of CD148 in fibroblasts. Syndecan-2

(SDC2) via binding its receptor protein tyrosine phosphatase CD148/PTPRJ activates an anti-fibrotic

pathway dependent on downregulation of TGF-β1-dependent signaling. TGF-β1 stimulates pro-fibrotic

effects via its receptor TGFβ-I/-II complex which activate a PI3K/AKT/mTOR-dependent signaling

pathway culminating in the suppression of autophagy. The autophagy pathway, driven by LC3-

dependent formation of autophagosomes, directs the lysosomal degradation of autophagosome-

sequestered cargo. Impaired autophagy is a characteristic feature of pulmonary fibrosis, which leads

to aberrant accumulation of the autophagy substrate and cargo adaptor protein p62. Accumulated

p62 promotes phosphorylation of the IKK complex, leading to phosphorylation and dissociation of I-

κB from the p65 subunit of NF-κB. The latter promotes p65/p50 assembly and migration of the NF-☐B

complex to the nucleus, where it stimulates pro-fibrotic gene expression. NF-κB has also been implicated in apoptosis resistance and myofibroblast differentiation, characteristic of the pro-fibrotic phenotype.   Sequences (*upper right*) depict an 18-aa peptide region of the SDC2 ectodomain (SDC2-pep) with a high degree of homology between human and mouse sequences. SDC2-pep was tested in the current study as a therapeutic ligand of CD148/PTPRJ and found to have anti-fibrotic effects in IPF and models of pulmonary fibrosis**.**

Supplementary Information: Materials and methods

Reagents

Antibodies against α-SMA (no. ab5694), collagen 1 (no. ab34710) and GAPDH (no. ab8245) were from Abcam. CD148/DEP1 (no. MAB1934) was from R&D systems. Hemagglutinin tag (HA-tag, no. G036) was from ABMgood (Richmond, BC, Canada). Antisera against phospho-Akt (Ser473, no. 9271), Akt (no. 9272), phospho-PI3K (p85 (Tyr458)/p55 (Tyr199), no. 4228), PI3K (p85, no. 4292), phospho-mTOR (Ser2448, no. 5536), mTOR (no. 2972), phospho-S6 ribosomal protein (Ser235/236, no. 2211), S6 ribosomal protein (no. 2217), phospho-p70 S6 kinase (Thr389, no. 9206), p70 S6 kinase (no. 2708), LC3a/b (no. 4108), p62 (no. 5114), phospho-IKKα/β (Ser176/180, no. 2697), IKKα (no. 2682), phospho-IκB-α (Ser32, no. 2859), I-κB-α (no. 4812), NF-κB (p65, no. 8242), β-actin (no. 4970), PCNA (no. 13110) were from Cell Signaling Technologies (Beverly, MA). All other reagents, including 4-hydroxy-tamoxifen, were from Millipore Sigma (St Louis, MO).

Primary Pulmonary Fibroblasts

This study was approved by the institutional review board at Brigham and Women's Hospital (approval number: 2011P002419). Lung fibroblasts were derived from patients who were subjected to lung transplantation with progressing IPF. Primary control lung (control) fibroblasts were derived from nonfibrotic lung samples lacking any evidence of disease which were deemed unsuitable for transplantation. Mouse lung fibroblasts from $Ptprj^{fl/fl}$ Col1a2-Cre-ER(T)$^{+/0}$, Col1a2-Cre-ER(T)$^{+/0}$ or GFP-LC3 transgenic mice were obtained as previously described (22). Briefly, isolated lungs were minced and digested in collagenase buffer. Cell pellets will be resuspended and cultured for 7-10 days. Cells were lineage and Sca-1 depleted using commercially available kits from StemCell Technologies (Vancouver, BC) to remove hematopoietic and progenitor cell populations. Fibroblasts were cultured in complete media (DMEM; Corning) containing 10% FBS (Corning), 100 IU of penicillin and 100 μg/ml streptomycin (Corning), 292 μg/ml L-glutamine (Corning), and 100 μg/ml Primocin (InVivoGen) in humidified incubators at 37°C and 10% CO_2. To induce Cre recombinase expression in $Ptprj^{fl/fl}$/Col1a2-Cre-ER(T)$^{+/0}$ or Col1a2-Cre-ER(T)$^{+/0}$ lung fibroblasts, cells were treated with 4-hydroxytamoxifen (4-OHT, 1 μM).

Histopathology and Immunofluorescent co-staining

Human lung sections were fixed by inflation with buffered 10% formalin solution and embedded in paraffin. Thin (4 μm)

sections were deparaffinized and rehydrated. Slides were boiled in 10 mM citrate buffer for α-SMA and CD148. Sections were incubated with anti-α-SMA antibodies (Abcam, Cambridge, MA, no. ab5694) and for anti-CD148 antibodies (R&D systems, Minneapolis, MN, no. MAB1934) overnight at 4°C. Species-matched fluorescent-conjugated secondary antibodies were applied for staining at 37°C for 1 h. Nuclei were stained with 4', 6-diamidino-2-phenylindole (DAPI). The slides were analyzed using an Olympus Inverted System Microscope IX70 (Olympus, Center Valley, PA), and photomicrographs were taken with a Nikon camera. CD148 fluorescence intensity was quantified by ImageJ. Mouse lungs were collected on Day 21, fixed with 4% (*wt/vol*) neutralized buffered paraformaldehyde, embedded in paraffin, and stained with hematoxylin and eosin (H+E) or Masson's trichrome.

Mice

All animal experimental protocols were approved by the Brigham and Women's Hospital Standing Committee for Animal Welfare. WT C57BL/6 mice were obtained from Charles River Laboratories and used at 8 weeks of age. GFP-LC3 transgenic mice (23) were kindly provided by Dr. Blumberg, Brigham and Women's Hospital, Boston, MA. Transgenic conditional PTPRJ/CD148-knockout mice of both sexes were bred as follows on a C57BL/6 background. Transgenic Col1a2$^{Cre-ER(T)+/0}$ and *Ptprj$^{fl/fl}$* mice were obtained from Jackson Laboratory (no. 029567, no. 008291 respectively, Bar-Harbor, ME). To generate fibroblast-specific CD148-deficient mice, *Ptprj$^{fl/fl}$* mice were bred with Col1a2$^{Cre-ER(T)+/0}$ (heterozygous allele) transgenic mice to generate mice heterozygous for both alleles. Progeny from the second cross between *Ptprj$^{fl/fl}$* mice and heterozygous *Ptprj$^{fl/WT}$* Col1a2$^{Cre-ER(T)+/0}$ mice (from the first cross) were used for further experiments. All mice were genotyped by PCR techniques as described previously. For treatment of mice, a stock solution of tamoxifen (Sigma-Aldrich) was diluted in corn oil to 20 mg/ml. To selectively delete CD148 in activated fibroblasts, adult *Ptprj*$^{fl/fl}$ Col1a2$^{Cre-ER(T)+/0}$ mice (8–10 weeks old) and control Col1a2$^{Cre-ER(T)+/0}$ mice were administered tamoxifen suspension (0.1 ml of diluted stock) *via* intraperitoneal (*i.p.*) injection (75 mg/kg), for 5 days before administration of BLM (0.75 mg/kg) and every 72 h thereafter until sacrifice as shown in Figure E15.

Bleomycin model of pulmonary fibrosis

Lung fibrosis was elicited in mice by intratracheal (*i.t.*) injection of a single dose of 0.75 mg/kg body weight of BLM (Cayman Chemical, Ann Arbor, MI); control mice received a volume of sterile saline equal to that described previously. Mice were sacrificed 21 days after BLM instillation. BAL fluids were collected to determine immune cell counts, and the

left lung was analyzed for hydroxyproline, while the right lung lobes were assessed for expression of fibrotic marker mRNAs (*Acta2*, *Col1a1*, *Tgfb1*, and *Ctgf*) and histology.

Hydroxyproline assay

To quantify collagen deposition, the left lung from each mouse was hydrolyzed in 6N HCl for 24 h at 110°C, and hydroxyproline levels were quantified as previously described (18). Each sample was tested in triplicate. Data are expressed as micrograms of hydroxyproline per left lung.

SDC2-ED 18-aa peptide (SDC2-pep) therapeutic administration

Ptprj$^{fl/fl}$ Col1a2$^{Cre-ER(T)+/0}$ (CD148 fibroblast-specific knockout) and Col1a2$^{Cre-ER(T)+/0}$ (control) mice at 8 weeks of age were treated with tamoxifen and instilled with 0.75 mg/kg of BLM in 100 µl sterile saline at Day 0. Control animals were treated with an equal volume of sterile saline. In the treatment group, SDC2-ED 18-aa peptide (SDC2-pep, 0.5 mg/kg in 50 µl of phosphate-buffered saline [PBS]) was administered at days 10, 12, 14, 16 and 18 post-BLM or saline by oropharyngeal instillation. The control group was treated with an equal volume of sterile PBS (vehicle). Mice were sacrificed 24 days after BLM or saline treatment.

Precision Cut Lung Slices (PCLS)

PCLS from control and IPF lungs were prepared as previously described (24, 25). Briefly, using a syringe pump, lungs were infiltrated with warm, 2% (37°C) low-melting agarose–HBSS solution (Millipore Sigma, no. A9414; kept at 37°C). After complete solidification of agarose in the inflated lobes on ice, tissue blocks of approximately 10 mm in diameter were prepared. Lung slices (300 µm thick) were cut perpendicularly to the visible airway with a vibratome (Precisionary Instruments, no. VF-300, Greenville, NC) at room temperature in HBSS. Then, slices were cultured in 24 well plates supplemented with DMEM/F12 media containing 1% FBS and antibiotics. Slices were transfected with scr, shCD148, EV or pLenti-GIII-CD148-HA lentiviral particles (1~1.5 MOI per slice). 12 h later, lung slices were incubated with or without SDC2-ED 18-aa peptide (5 µM) for another 72 h. After treatment, slices were subjected to total RNA isolation to measure profibrotic genes expression (*Acta2, Col1a1* and *Fn*) or immunofluorescent staining.

Western Immunoblot Analysis

Polyacrylamide gel electrophoresis and immunoblotting were performed according to standard methods as previously described (27). The electrophoresed proteins were transferred to polyvinylidene difluoride (PVDF) membranes by semidry electrophoretic transfer at 15 V for 60–75 min. The membranes were blocked overnight at 4°C in 5% bovine serum albumin (BSA). The cells were incubated with primary antibodies diluted 1:500 in Tris-buffered saline/Tween 20 (TBS-T) containing 5% BSA for 2 h and then incubated with the secondary antibody at room temperature for 1 h. Suitable horseradish peroxidase (HRP)-conjugated secondary antibodies were used (1:5000 dilution in TBST containing 1% BSA). The signals were detected by ECL (Thermo Fisher Scientific, Waltham, MA). Quantification of protein bands was performed with the computer software ImageJ (Image Processing and Analysis in Java Edition: 1.29 URL: http://rsb.info.nih.gov/ij/ NIH, Maryland) and was expressed as a ratio of band intensity with respect to the loading control.

Quantitative Real-Time PCR (qPCR)

Total RNA was isolated with Trizol reagent (Invitrogen, Carlsbad, CA) and cDNA was synthesized from RNA (1 μg) using a SuperScript First-strand synthesis system for reverse transcription (RT) PCR (Invitrogen, Carlsbad, CA). Primer sequences are shown in the Table S1. RT-PCR, with SYBR Green Master Mix (Bio-Rad Laboratories, Hercules, CA, USA), was performed using the StepOnePlus Real-Time PCR System (Applied Biosystems, Foster City, CA, USA). The relative quantity of target mRNA was calculated by use of the CT method, or $2-\Delta\Delta CT$, as described (27), and normalized by use of GAPDH as an endogenous control (Sequence Detection System software, version 1.7; Applied Biosystems).

Lentiviral Transfection

For CD148 silencing experiments, the pLKO.1 plasmid, carrying the human shRNA PTPRJ/CD148 target sequence ACGAGTCGTCATCTAACTATA (consortium number TRCN0000320555) and pLKO.1, carrying a Scr sequence, were purchased from Sigma-Aldrich. For CD148 overexpression pLenti-GIII-CD148-HA (no. LV278210) and empty vector (EV, pLenti-GIII-HA) plasmids were purchased from (ABMgood, Vancouver, BC). Lentiviral particles were generated by use of a commercially available packaging mix, provided by MilliporeSigma (no. SHP001) or by ABMgood (no. LV003) in human embryonic kidney 293 T cells, according to the manufacturer's instructions. Lentiviral particle containing media was harvested and concentrated using a Centricon Plus-70 Centrifugal Filter (no. UFC700308, Millipore Sigma, St Louis, MO). Lung fibroblasts were infected with the lentiviral particles, and stably infected cells were selected by use of puromycin (10 μg/ml).

Gel contraction assay

The assay was performed as previously described (18). Briefly, cell pellets of lung fibroblasts were mixed with 8 volumes of rat tail type I collagen suspension, one volume of 1X concentrated PBS and one volume of reconstitution buffer (2% sodium bicarbonate and 4.77% HEPES dissolved in 0.05 N NaOH) at a concentration of 2×10^6 cells/ml. Cell-populated collagen solution was immediately poured into a 24-well-plate (0.5 ml/well) and incubated at 37°C for 1 h to permit complete gelation. 16 h later, gels were gently transferred to 60 mm cell culture dish with a spatula and overlaid with culture media. Gel images were taken at 0, 12 and 24 h.

Fas ligand (FasL) treatment

Soluble recombinant human FasL was purchased from Enzo life sciences (Cat N: ALX-522-020) and dissolved in 1 x PBS. Cells were treated with FasL at doses of 100 or 200 ng/ml and incubated for 24 hours. After incubation cell viability was measured using MTT assay or subjected to caspase-3 activity assay as described below.

Cell viability

Cell viability was determined using the 3-[4,5-dimethylthiazol-2-yl]-2,5-diphenyl tetrazolium bromide (MTT) assay and trypan blue exclusion assay as previously described (26). Cells were seeded at 1×10^4 cells/well in 24-well plates. After different treatments, 20 μl of 5 mg/ml MTT solution was added to each well (0.1 mg/well), and wells were incubated for 4 h. The supernatants were aspirated, the formazan crystals in each well were dissolved in 200 μL of dimethyl sulfoxide for 30 min at 37°C, and optical density at 570 nm was read on a microplate reader. For the trypan blue exclusion assay, cells were harvested and 10 μL of 0.4% trypan blue solution was added to 10 μL of cells collected from each well, and the cells were incubated for 2 min. Unstained live cells were counted on an automated cell counter.

Caspase-3 activity assay

Caspase-3 activity in protein cell lysates were measured using a commercially available kit (no. K006-100, Biovision, San Francisco, CA).

Luciferase assay

3×10^5 cells/well were plated in triplicate on 6-well plates and incubated for 24 h. Transient transfection assays in cells were performed by use of FuGENE 6 transfection reagent (Promega, Madison, WI), as described previously (26). The construct carrying five copies of an NF-κB response element that drives transcription of the luciferase reporter gene (Promega, Madison, WI, no. 9PIE849, 500 ng/well) and a β-galactosidase expression plasmid (250 ng/well) to correct for transfection efficiency were co-transfected into mouse lung fibroblasts. The cells were harvested for luciferase activity using the Luciferase Assay System (Promega, Madison, WI), 6 h after treatment with TGF-β1 (10 ng/ml). Luciferase activity was measured in a Wallace Victor3 1420 multilabel counter (PerkinElmer, Waltham, MA). β-Galactosidase activity was measured using the mammalian β-Galactosidase Assay Kit (Thermo Fisher Scientific, Waltham, MA).

CD148 gene expression analysis in single cell RNA sequencing (scRNA-seq) dataset

From a published scRNA-seq dataset (29), clusters labeled fibroblast and myofibroblast were extracted for analysis. Pseudo-samples were generated by summing all the counts matrices for a given patient sample within the cluster. A differential pseudo-bulk expression analysis comparing IPF over controls was performed using a negative binomial generalized linear model as implemented for EdgeR in the R- statistical programming environment.

Statistical analysis

Data are expressed as mean ± SEM. Comparisons of mortality were made by analyzing Kaplan-Meier survival curves and log-rank tests to assess for differences in survival. For comparisons between two groups, we used Student's unpaired t test or Mann-Whitney's non-parametric test. Statistical significance was defined as $P<0.05$. One-way analysis of variance, followed by Newman-Keuls or Tukey's post-test analysis, or Kurskal-Wallis non-parametric test, was used for analysis of more than two groups. The numbers of samples per group (n), or the numbers of experiments, are specified in the figure legends.

Supplementary Figures
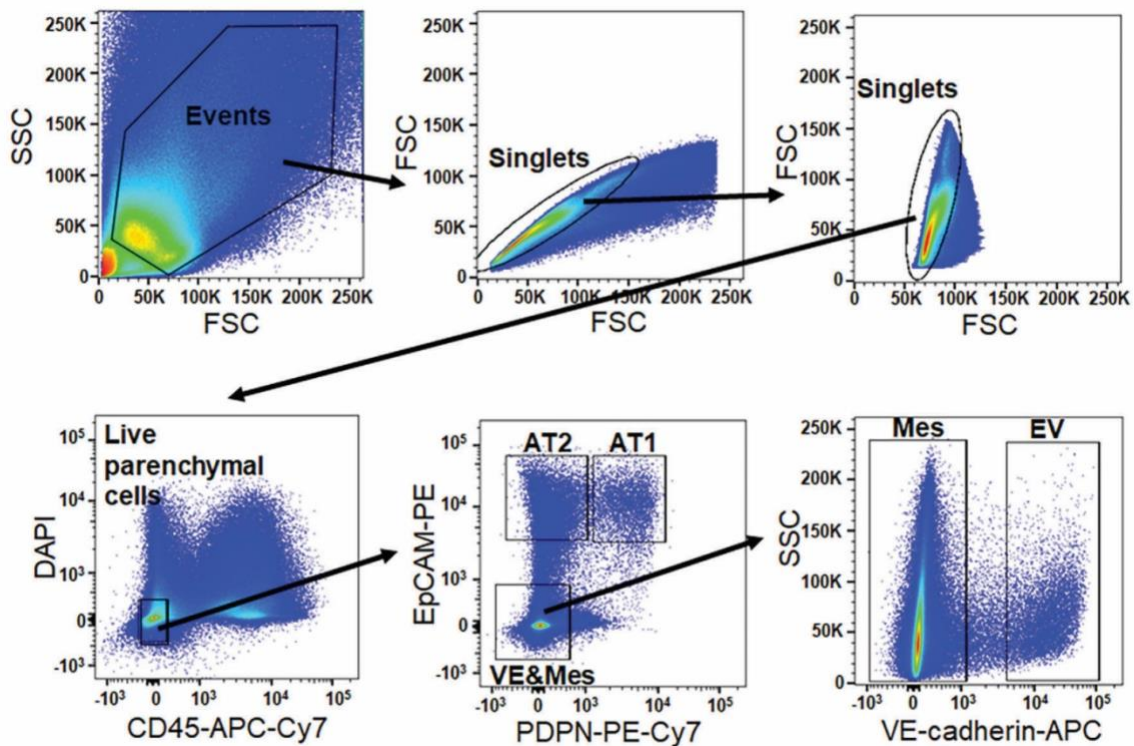
Fig. E1. Sorting of lung epithelial and mesenchymal cells. Lung tissue from control or IPF lungs were digested in collagenase buffer. Cells were stained with DAPI, CD45-APC-Cy7, EpCAM-PE, PDPN-PE-Cy7 and VE-cadherin-APC. The AT1 population was defined as Live/CD45^{neg}/EpCAM^{pos}/PDPN^{pos}. The AT2 population was defined as Live/CD45^{neg}/EpCAM^{pos}/PDPN^{neg}, Mesenchymal (fibroblast-enriched) cells were defined as Live/CD45^{neg}/EpCAM^{neg}/PDPN^{neg}/VE-cadherin^{neg}.
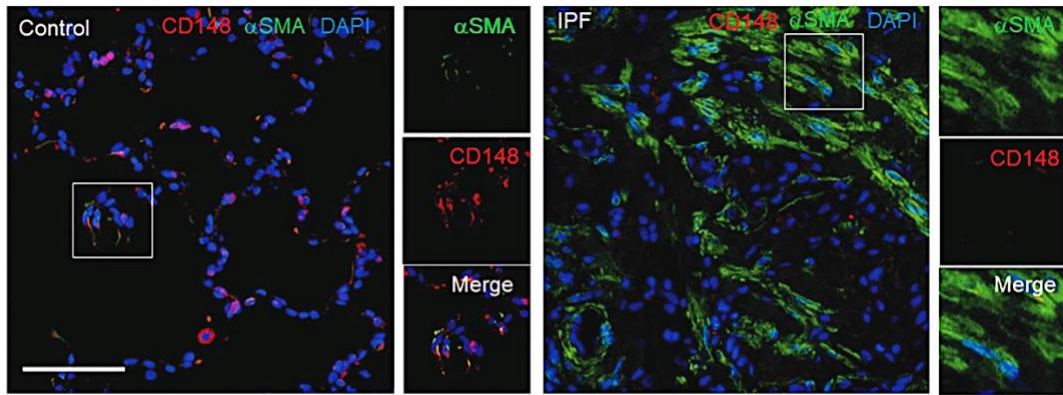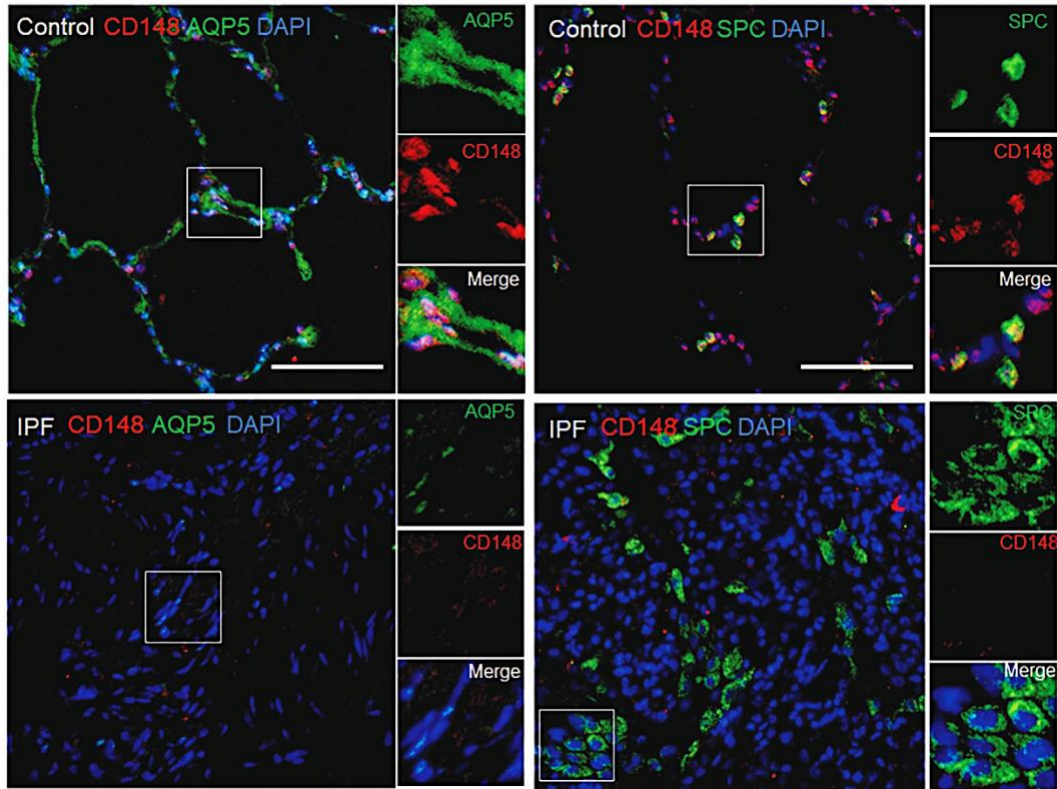
Fig. E2. CD148 is not expressed in myofibroblasts; but is expressed in alveolar epithelial cells and downregulated during fibrosis. (**A**) Digital images of CD148 (Cy3, red), αSMA (GFP, green) and DAPI (blue) in control (*left*) and IPF (*right*) lung tissue. (**B**) Digital images of CD148 (Cy3, red), AQP5 (GFP, green) and DAPI (blue) in control and IPF lung tissue (*left panels*); or CD148 (Cy3, red), SPC (GFP, green) and DAPI (blue) in control and IPF lung tissue (*right panels*) were taken using fluorescent microscopy. Representative images from 3 controls and 4 IPF are shown (scale bar = 100 μm).
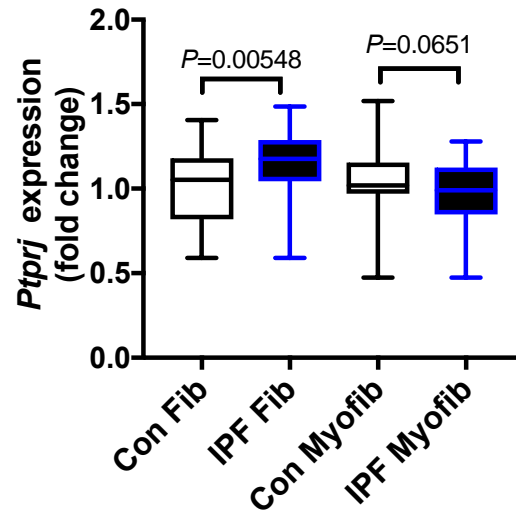
Fig. E3. CD148 gene expression in fibroblasts and myofibroblasts from single cell RNA sequencing (scRNA-seq). Clusters labeled as fibroblast and myofibroblast were extracted from our previously published scRNA-seq data set (29) and analysed using R-program. Data are presented as box and whiskers plot. *P* values were calculated by Mann-Whitney unpaired test.
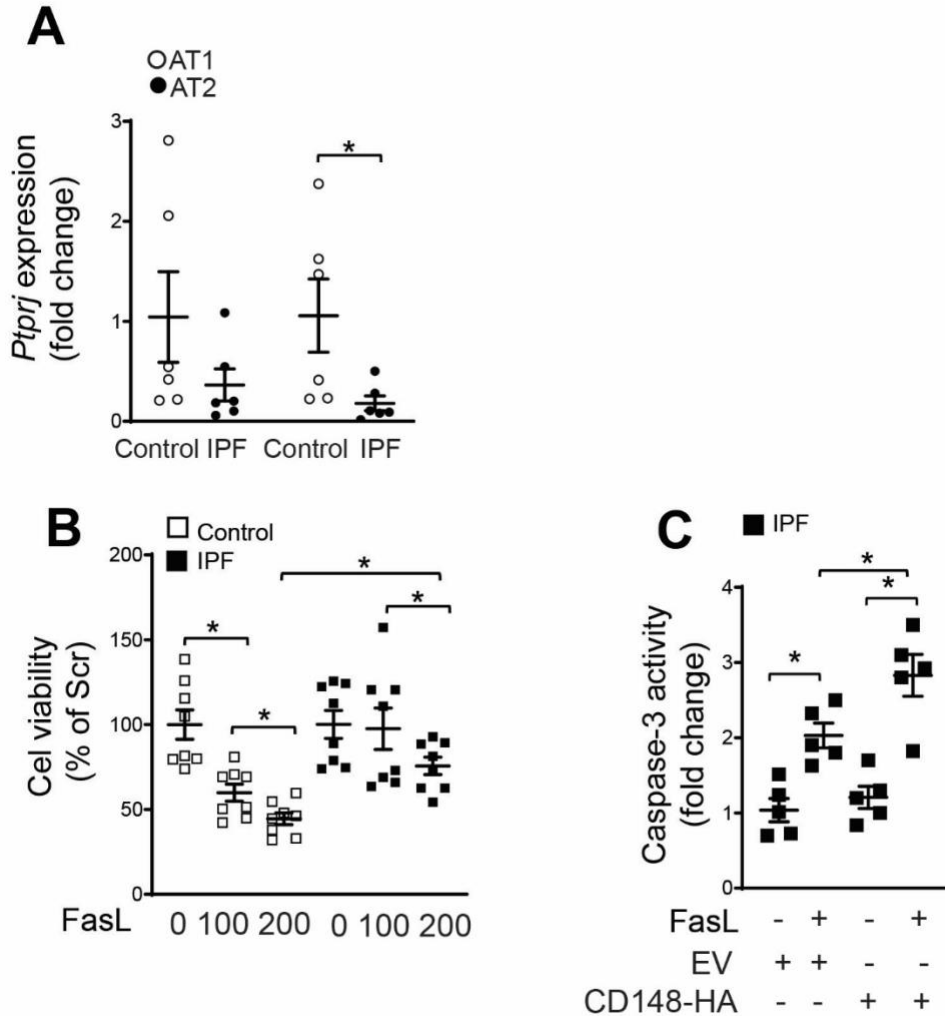
Fig. E4. CD148 is downregulated and alveolar epithelial cells during fibrosis; and regulates caspase-3 activity in IPF fibroblasts. (A) mRNA expression of CD148 in sorted AT1 and AT2 cells were assessed using qPCR. (**B**) Control and IPF derived lung fibroblasts were seeded at equal amount in 24 well plates and then treated with Fas ligand (FasL) (100 and 200 ng/ml) for 24 h. After treatment, cell viability was assessed with the MTT assay (*n*=4). (**C**) EV and CD148-HA transfected cells were seeded at equal amount in 24 well plates and treated with FasL (200 ng/ml) for 24 h. After treatment, cells were subjected to caspase-3 activity assay (*n*=5). Data are mean ± s.e.m. *P<0.05, by Student's unpaired t test for A and one-way ANOVA for B,C.
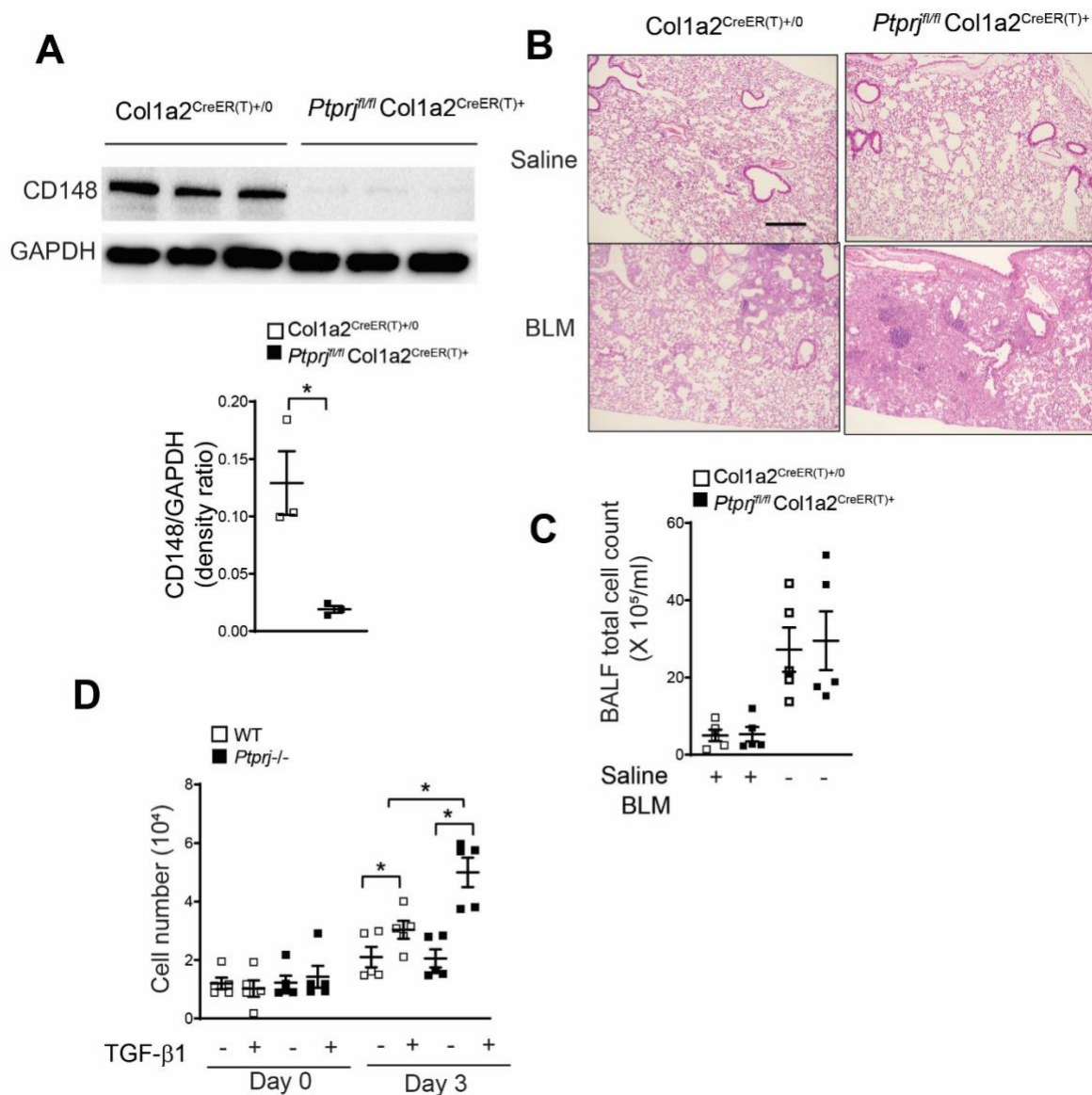
Fig. E5. CD148 deficiency in fibroblasts does not affect lung inflammation after BLM injury but regulates cell growth after TGF-β1 stimulation. (**A**) *Ptprj*^fl/fl Col1a2^Cre-ER(T)+/0 mice (fibroblast-specific CD148 deficient) and Col1a2^Cre-ER(T)+/0 (WT) mice were treated with tamoxifen (75 mg/kg, *i.p.*), once a day for 5 days. Then, lung fibroblasts were isolated and plated. 5 days later, cells were lysed and subjected to western blot to measure CD148 expression (*n*=3). (**B**) Col1a2^Cre-ER(T)+/0 mice (fibroblast-specific CD148 deficient) and Col1a2^Cre-ER(T)+/0 (WT) mice were exposed to BLM to induce lung fibrosis. 21 days later, mouse lungs were harvested and stained with hematoxylin and eosin (H&E) on the same area shown for Trichrome staining in Figure 2a. (**C**) Total cell concentrations were measured in BAL fluid 21 days after BLM injury (*n*=5). (**D**) WT and *Ptprj*^-/- mouse lung fibroblasts were harvested and plated at 1x10^4 cells/well in the presence or absence of TGF-β1 (10 ng/ml). 3 days later, cells were harvested, and live cells were estimated using the trypan blue exclusion assay, as described in Supplemental Methods (*n*=3). Data are mean ± s.e.m. *P<0.05, by Student's unpaired t test for A and one-way ANOVA for C.
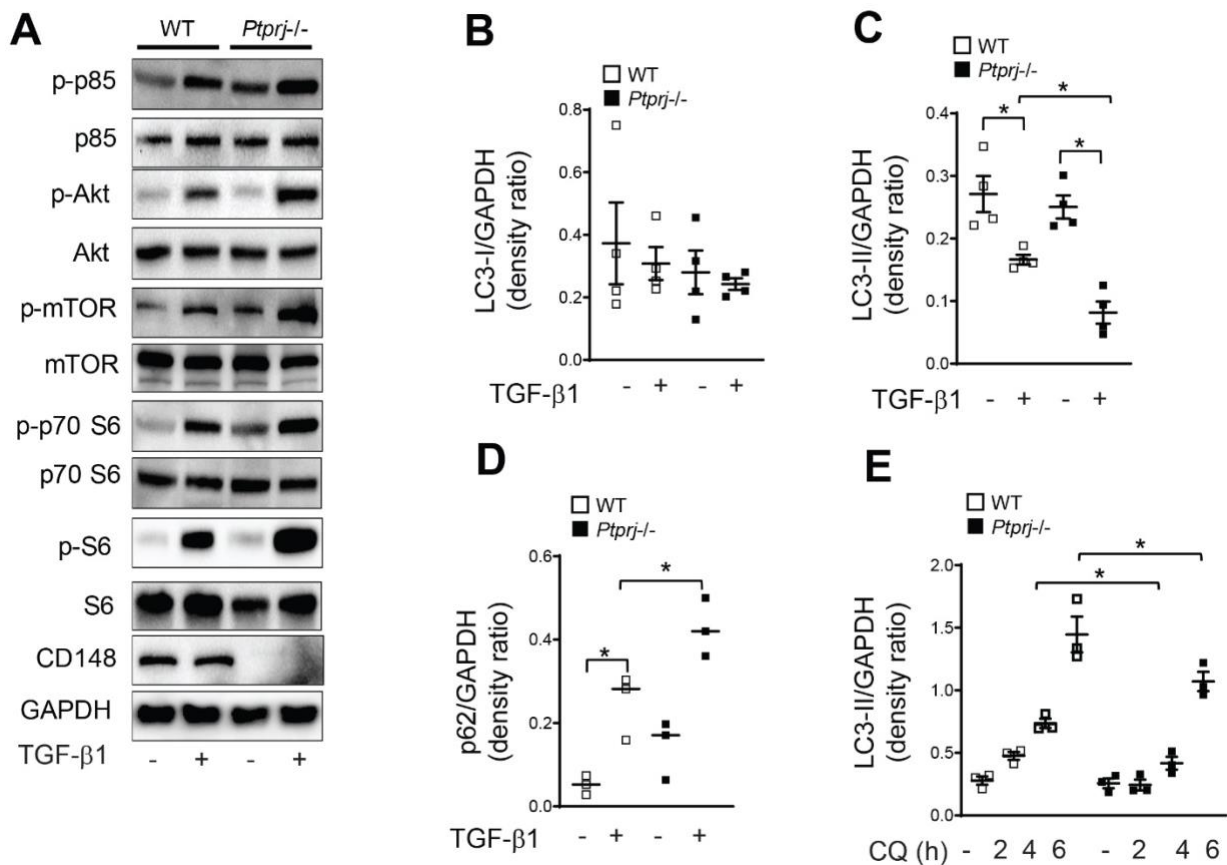
Fig. E6. Supplementary immunoblot data and densitometry analyses. (A) Mouse lung fibroblasts were isolated from *Ptprj*^fl/fl Col1a2^Cre-ER(T)+/0 mice (*Ptprj*^-/-) and Col1a2^Cre-ER(T)+/0 mice (WT) and then treated with 4-OHT (1 μM) for 24 h. After 4-OHT treatment, cells were exposed to TGF-β1 (10 ng/ml) for 24 h. After stimulation, cells were harvested, and the expression of p-p85 (Tyr458), p-Akt (Ser473), p-mTOR (Ser2448), p70 S6 kinase (Thr389), p-S6 ribosomal protein (Ser235/236) and CD148 (*n*=4 for each condition) in lysates was determined by Western analysis, (Corresponding to Densitometry analysis shown in Figure 3A).   Quantification of band intensity of target proteins (**A**) LC3I, (**B**) LC3-II, (**C**) p62 (corresponding to Western in Figure 3C) or (**D**) LC3II (corresponding to Western blot in Figure 3D). Band intensities were quantified using ImageJ software and was expressed as the ratio of band intensity to GAPDH. Data are mean ± s.e.m. *P<0.05, by one-way ANOVA.
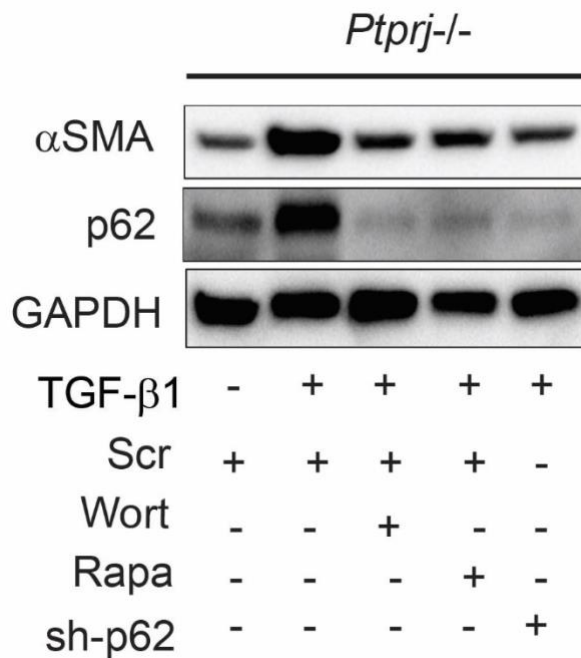
Fig. E7. Increase of ECM expression in CD148-deficient cells in response to TGF-β1 is dependent on the PI3K/mTOR axis and p62. *Ptprj*[/-] cells were transfected with scr or shp62 (lentivirus). Cells were stimulated with TGF-β1 (10 ng/ml) in the presence or absence of wortmannin (wort, 50 nM) or rapamycin (rapa, 1 μM). 24 h cells were lysed, and subjected to western blot (α-SMA, *n*=3). GAPDH was the standard.
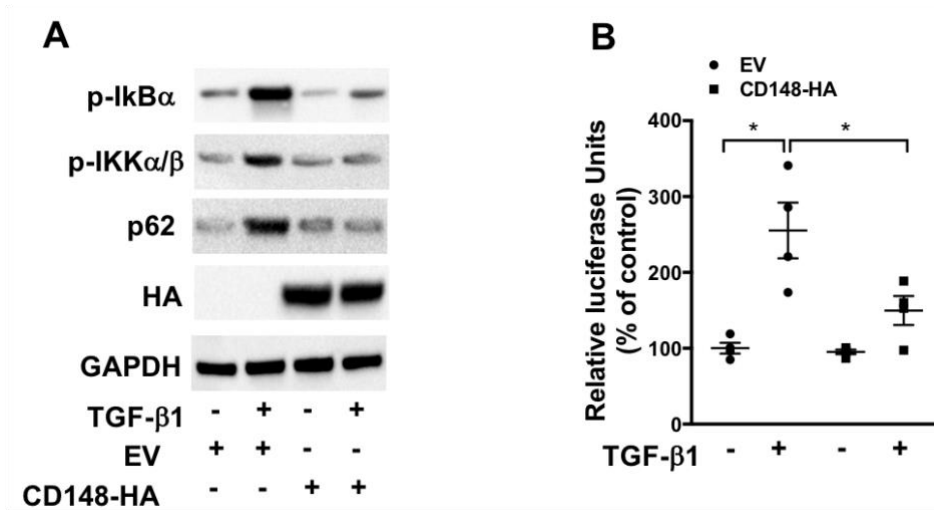
Fig. E8. CD148 overexpression inhibits NF-κB activation and p62 expression. (**A**) Human lung fibroblasts (MRC-5 cells) were lentivirally transfected with empty vector (EV, pLenti-GIII-HA) or pLenti-GIII-CD148-HA (CD148-HA). Then cells were stimulated with TGF-β1 (10 ng/ml) for an additional 24 h. After stimulation, cells were harvested and lysates were subjected to western blot to measure p-IKKα/β, p-IκB and p62 (*n*=3). (**B**) EV and CD148-HA transfected MRC-5 cells were additionally transfected with NF-κB luciferase reporter plasmid. Then, cells were treated with TGF-β1 (10 ng/ml) for 4 h. After stimulation luciferase activity was measured as described in methods (*n*=4). Data are mean ± s.e.m. *$P<0.05$, by one-way ANOVA.
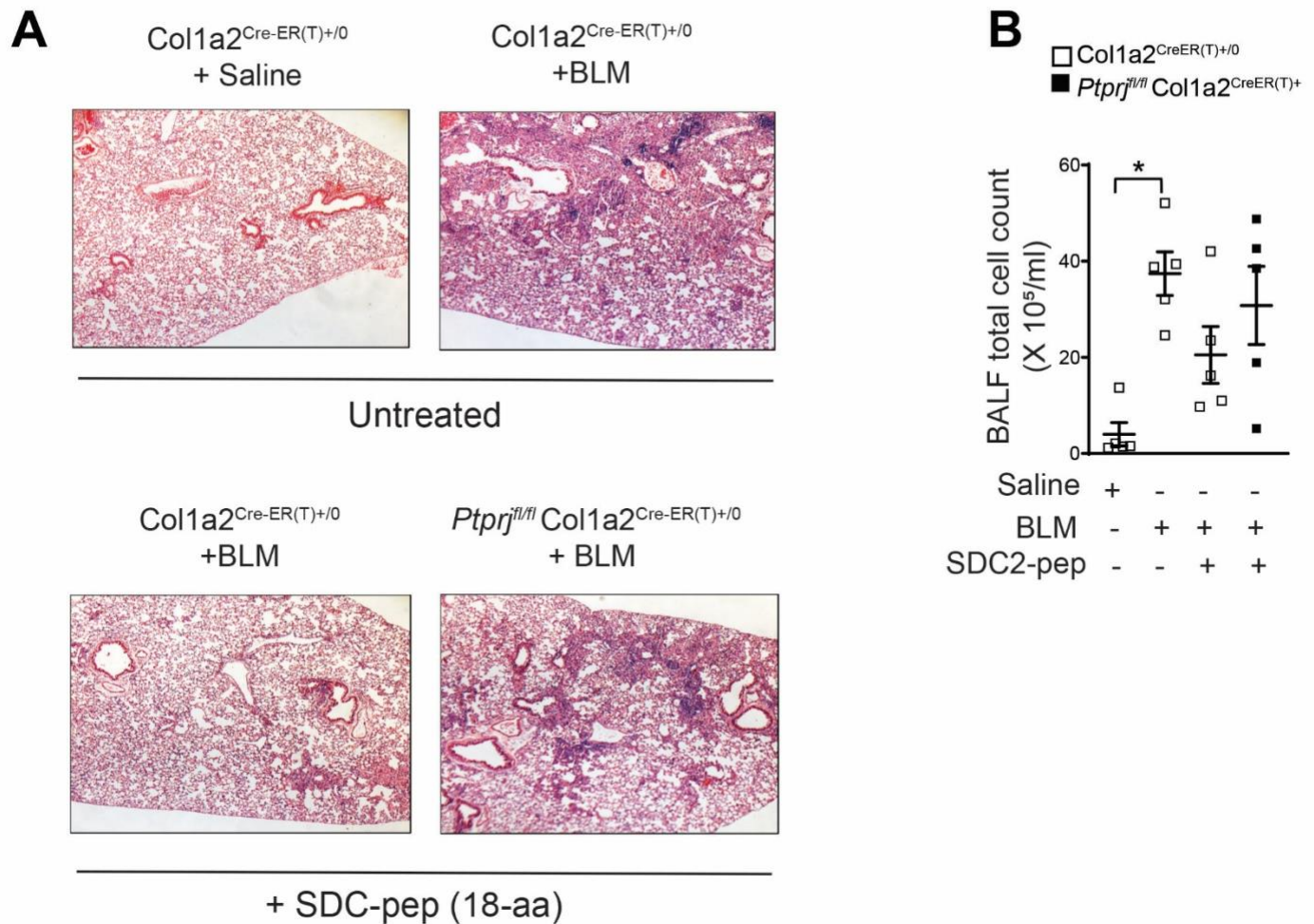
Fig. E9. SDC2-pep alleviates lung fibrosis after BLM-induced injury. *Ptprj*^{fl/fl} Col1a2^{Cre-ER(T)+/0} mice (fibroblast-specific CD148 deficient) and Col1a2^{Cre-ER(T)+/0} (WT) mice were exposed to BLM. SDC2-pep (0.5 mg/kg) was intranasally delivered into WT and *Ptprj*^{fl/fl} Col1a2^{Cre-ER(T)+/0} mice 10 days after BLM injury. Treatments were repeated at day 12, 14, 16 and 18. At 21 days after BLM exposure lungs were harvested and (**A**) images from hematoxylin and eosin (H&E) stained tissue were taken for the same area as shown for trichrome staining shown in Figure 6A. (**B**) Total cell concentrations were measured in BAL fluid from *Ptprj*^{fl/fl} Col1a2^{Cre-ER(T)+/0} mice and Col1a2-Cre (control) mice 21 days after BLM injury (*n*=5/group).
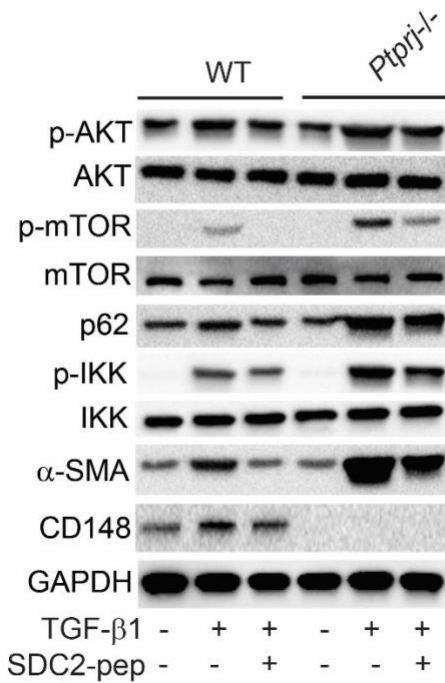
Fig. E10. Representative Western Blot. Mouse lung fibroblasts from *Ptprj^fl/fl* Col1a2^Cre-ER(T)+/0 mice (*Ptprj^-/-*) and Col1a2^Cre-ER(T)+/0 mice (WT) were isolated and treated with 4-OHT (1 μM) for 24 h. After 4-OHT treatment, cells were exposed to TGF-β1 (10 ng/ml) for an additional 24 h, in the absence or presence of SDC2-pep (5 μM). Expression of indicated markers p-AKT, Akt, p-mTOR, mTOR, p62, p-IKKα/β, IKKα, α-SMA, CD148. GAPDH was the standard (Corresponding Densitometry is shown in Fig. 5E of the main manuscript).
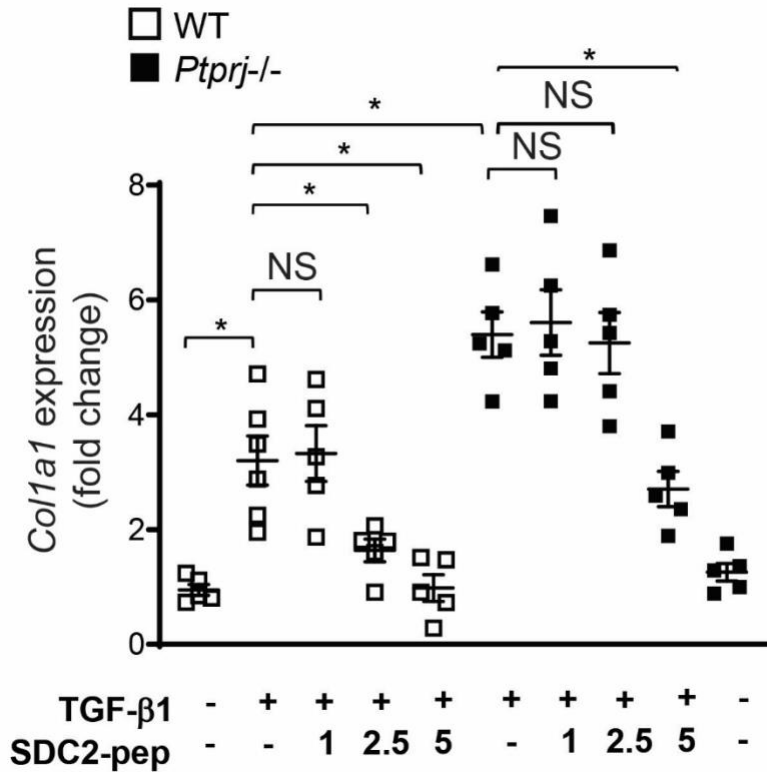
Fig. E11. SDC2-pep inhibits collagen1a1 expression in dose-dependent manner. *Ptprj*^{fl/fl} Col1a2[Cre-ER(T)+/0] (*Ptprj-/-*) or Col1a2[Cre-ER(T)+/0] (wild type) isolated fibroblasts were treated with 4-OHT (1 μM) for 24 h. Then, cells were stimulated with TGF-β1 (10 ng/ml) for an additional 24 h in the presence or absence of SDC2-pep (1, 2.5, 5 μM). After stimulation, total RNA was harvested with Trizol and subjected to qPCR to measure collagen1a1 (*Col1a1*) (n=5-6). Data are mean ± s.e.m. *$P<0.05$, by one-way ANOVA.
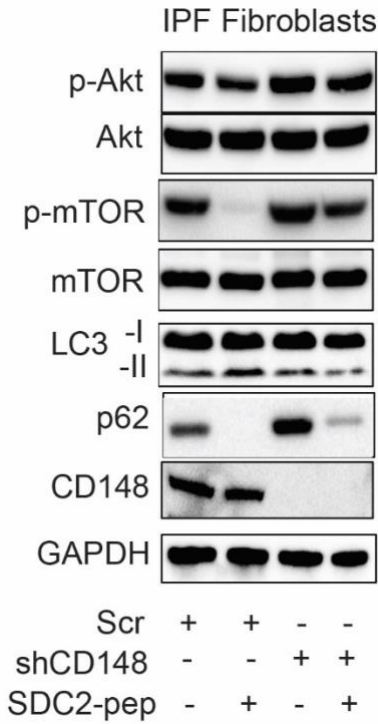
Fig. E12. Representative Western blot. IPF-derived lung fibroblasts were transfected with scr or shCD148. Then cells were treated with SDC2 18-aa peptide (5 μM) for 24 h. After incubation, p-Akt (Ser473), p-mTOR (Ser2448), LC3, p62 and CD148 were measured by western blot. GAPDH was the standard. (Corresponding Densitometry is shown in Fig. 6A of the main manuscript).
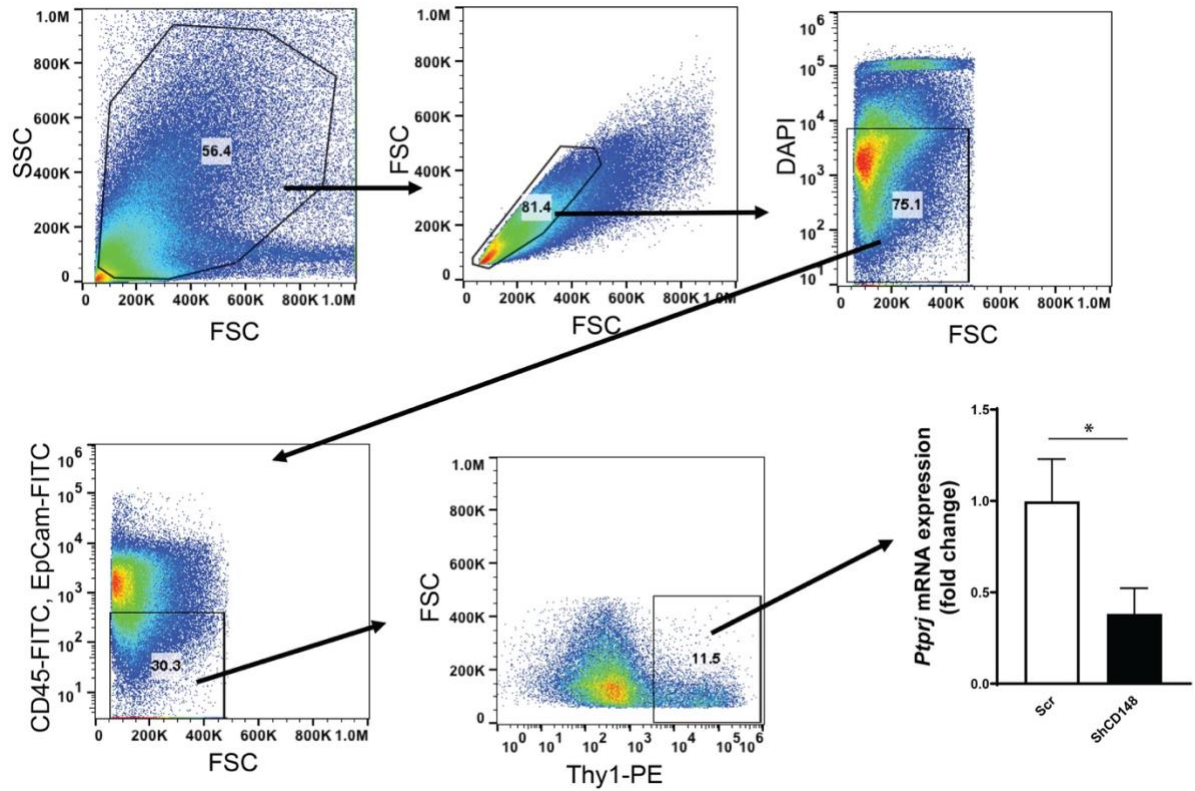
Fig. E13. shCD148 downregulates CD148 expression in PCLS-sorted fibroblasts. PCLS from an IPF patient were transfected with Scr (*n*=3) or ShCD148 (*n*=3) lentiviral particles as described in Methods. 72 hours after transfection, PCLS were digested to a single cell suspension and subjected to CD45-FITC, EpCam-FITC, Thy-1-PE and DAPI staining. The CD45^neg/EpCam^neg/Thy-1^pos population was considered as fibroblasts. *Ptprj* gene expression was determined by RT-PCR. Data are mean ± s.e.m. *P<0.05, by Student's t-test.
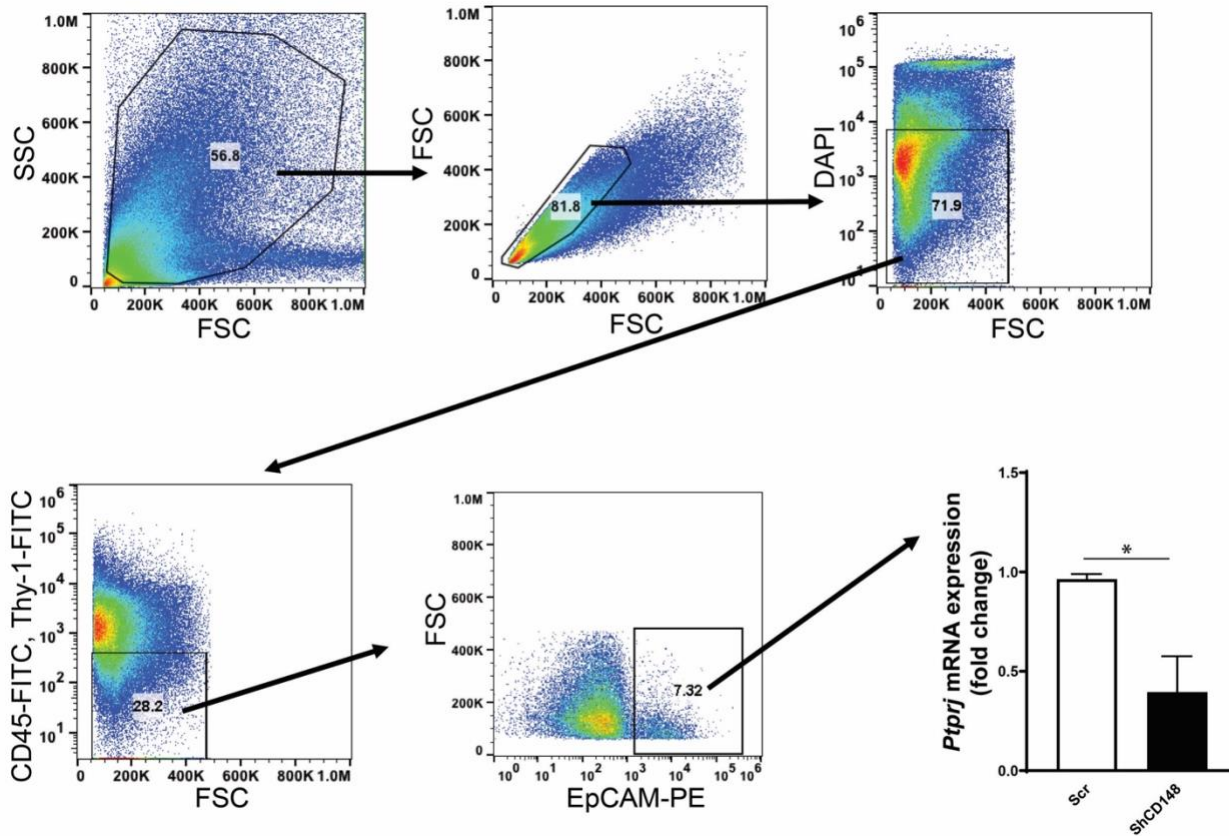
Fig. E14. shCD148 downregulates CD148 expression in PCLS-sorted epithelial cells. PCLS from an IPF patient were transfected with Scr (*n*=3) or ShCD148 (*n*=3) lentiviral particles as described in Methods. 72 hours after transfection, PCLS were digested to single cell suspension and subjected to CD45-FITC, Thy-1-FITC EpCam-PE, and DAPI staining. The CD45^{neg}/Thy-1^{neg}/EpCam^{pos} population was considered as epithelial cells. *Ptprj* gene expression was determined by RT-PCR. Data are mean ± s.e.m. *P<0.05, by Student's t-test.
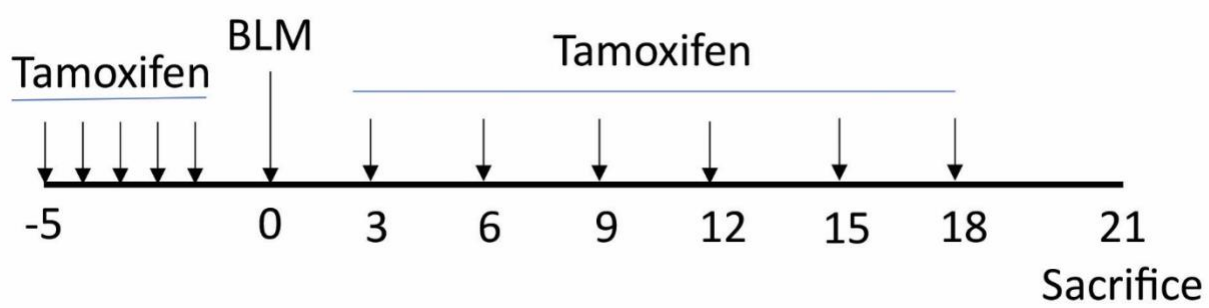
Fig. E15. Schematic overview of Tamoxifen treatments to induce conditional knockout of CD148 in fibroblasts.